ABSTRACT

STOCKING, CASEY L. An Investigation on the Impact of Temperature and Density Homogenization on Vessel Fluence Calculations. (Under the direction of Maria Avramova and Dave Kropaczek.)

As the reactor fleet continues to age, accurately modeling the reactor pressure vessel fluence becomes necessary for estimating radiation embrittlement. The majority of previous work in this field has been conducted using deterministic neutronic codes. This work focuses on core approximation methods that allow for Monte Carlo vessel fluence results at a reasonable computational expense. This investigation was performed using VERAShift; a code within the VERA code suite. VERAShift is comprised of a coupled eigenvalue calculation between MPACT, a deterministic neutronics code, and CTF, a subchannel thermal-hydraulic code. The fission source, temperatures, and densities are then passed to Shift, a continuous-energy Monte Carlo radiation transport code, which performs a fixed source vessel fluence calculation.

The objective of this thesis is to investigate core approximation techniques. Specifically, this thesis investigates the impact of various temperature and density homogenizations in a reactor core on vessel fluence calculations. These homogenizations are intended to reduce memory usage while maintaining accuracy. There are two main homogenization types being considered; assembly-averaged and ring-averaged. Assembly averaged homogenization performs volume-averaged temperature and density homogenization over each assembly and ring-averaged homogenizations are performed over radial rings about the center of the core. The explicit peripheral fuel pins option allows for explicit temperature and density modeling in the outer most pincells and assemblies. Semi-unique pincells were created to reduce the memory usage for homogenizations by using fewer unique pincell descriptions.

The Consortium for Advanced Simulation of Light Water Reactors Advanced Modeling Applications Problem 7 was used to benchmark the core approximation techniques investigated in this thesis. This problem models a beginning of life reactor at hot full power. Two problem configurations are considered; a full quarter-core model and a mini quarter-core model. The full model is based on Watts Bar Unit 1; a Westinghouse 4 loop pressurized water reactor. The mini-core model was developed by the Consortium for Advanced Simulation of Light Water Reactors for benchmarking MPACT and is a scaled down version of the Watts Bar reactor with 7x7 assemblies and a 9x9 core.

Seven cases were considered for comparing the accuracy of semi-unique pincells and unique pincells. These cases showed good agreement between semi-unique and unique pincell configurations. This showed that semi-unique pincells accurately model the reactor geometry for vessel fluence calculations. Eleven mini-core cases were chosen for investigating the accuracy of temperature and density homogenization in vessel fluence calculations. All of the homogenizations investigated were significantly more accurate than the nonunique pincell model. Pin-ring homoge-

nizations performed inconsistently; depending on ring thickness and location. It was hypothesized this is caused by lumping varying enrichments together. These homogenizations were also shown to provide moderate to significant performance enhancements; up to a factor of 2-3 reduction in memory and a factor of 5 reduction in runtime. All of the homogenizations were also shown to out-perform nonunique pincells for a realistic reactor geometry. Overall, temperature and density homogenization using semi-unique pincells appears extremely promising.

An Investigation on the Impact of Temperature and Density Homogenization on Vessel Fluence Calculations

by
Casey L. Stocking

A thesis submitted to the Graduate Faculty of
North Carolina State University
in partial fulfillment of the
requirements for the Degree of
Master of Science

Nuclear Engineering

Raleigh, North Carolina

2018

APPROVED BY:

Maria Avramova Co-chair of Advisory Committee	Dave Kropaczek Co-chair of Advisory Committee

Ralph Smith

DEDICATION

To my parents.

BIOGRAPHY

Casey Stocking was raised from a young age in Durham, NC. From a young age he was fascinated in science and the way things worked. He came to NC State in 2012 to begin a bachelor's degree in Nuclear Engineering. Graduating in 2016, Casey decided to remain at NC State; pursuing an MS in nuclear engineering. His research, under Dr. Maria Avramova and mentored by Dr. Tara Pandya from ORNL, focused on code development for Shift.

Outside of school, Casey is an avid NC State football and basketball fan. He enjoys attending games with friends and cheering on the pack. He enjoys hiking and exploring with his girlfriend Rosie and dog Simba.

ACKNOWLEDGEMENTS

I would first like to thank my friends and family who have supported me throughout my educational career. I never could have done this without your help and constant support.

I would like to thank Dr. Tara Pandya for all of your help and guidance in completing my research. Without your knowledge and support I would not have been able to accomplish this feat. Additionally, I would like to thank Dr. Avramova for all of her help and support. Our weekly meetings kept me on track and your advice was crucial to this work.

This research was supported by the Consortium for Advanced Simulation of Light Water Reactors (http://www.casl.gov), an Energy Innovation Hub (http://www.energy.gov/hubs) for Modeling and Simulation of Nuclear Reactors under U.S. Department of Energy Contract No. DE-AC05-00OR22725. This research was also supported by Oak Ridge National Laboratory (ORNL), which is managed and operated by UT-Battelle, LLC, for the U.S. Department of Energy (DOE) under the same contract number.

TABLE OF CONTENTS

LIST OF TABLES

LIST OF FIGURES

CHAPTER

1

INTRODUCTION

As the current reactor fleet ages, reactor vessel fluence determinations are becoming increasingly important in ensuring the integrity of pressure vessels. After years of exposure to a high flux of neutrons, the reactor pressure vessel has been weakened due to radiation embrittlement. Accurately determining the pressure vessel neutron fluence throughout the life of the plant can assist in approximating the vessel fracture toughness.

The majority of work on vessel fluence calculations to this point has used deterministic neutronic codes. This is largely due to the computational expense of Monte Carlo methods for large and complicated models. As a result of few particles reaching the pressure vessel, Monte Carlo calculations require long computational times to achieve acceptably low statistical uncertainty for excore calculations. Variance reduction methods can be utilized to reduce computational times, but these times remain longer than for deterministic methods. In addition to long computational times, memory usage becomes restrictive for large detailed geometry. This research is intended to implement and test core approximation techniques to reduce memory usage.

The goal of this thesis is to investigate core approximation methods and their impact on vessel fluence calculations. Specifically, we evaluated temperature and density homogenization in the fuel, cladding, and moderator. These are intended to reduce memory usage by using fewer unique geometry and material specifications.

Chapter 1 gives an introduction to the codes that were used in this research and previous work in this field. Chapter 2 introduces the homogenization types, current geometry specifications, and

a new geometry option. Chapter 3 presents the Consortium for Advanced Simulation of Light Water Reactors(CASL) Advanced Modeling Applications(AMA) problem 7, including a mini-core and full quarter core model; used to benchmark these homogenization methods. Chapter 4 presents the results of this investigation. These results investigate the use of semi-unique pincells and the impact of various homogenization methods. Chapter 5 discusses the conclusion of this research and possible future work.

Literature Review

Due to computational limitations, such as long computational times and large memory usage, there has not been a great deal of work performed in the realm of Monte Carlo vessel fluence calculations. The majority of previous work has been accomplished using deterministic neutronics codes.

NRC Vessel Fluence Regulatory Guide

In 2001, the Nuclear Regulatory Commission (NRC) released their guidelines for determining pressure vessel neutron fluence values[1]. This regulatory guide was developed and published to provide state-of-the-art methods to calculate and measure pressure vessel fluence that is accepted by the NRC. These guidelines are intended to ensure the accuracy and reliability of the fluence determination, required by 10 CFR Part 50, by providing methods and assumptions acceptable to NRC staff. These guidelines are intended for use only for Light Water Reactors. Compliance with these guidelines is not a regulatory requirement, but provides a blueprint for licensees to follow.

In determining the vessel fluence, the neutron flux must be calculated from the core out to the vessel and cavity. These calculations consist of the following steps:

1. Determine the geometrical and material input data.
2. Determine the neutron source.
3. Propagate the neutron source to the vessel and cavity.
4. Qualify the calculational methods.

Detailed geometry and material specifications should be used to accurately model the physical conditions within the reactor system. These specifications should include, material compositions, regional temperatures, and the complete geometry. All geometrical data should be based on documented plant dimensions. Water number densities should be based on full-power operating temperatures and pressures; accounting for axial and radial density variations due to temperature differences. Additionally, neutron reaction cross sections should be created from the latest available version of the Evaluated Nuclear Data File(ENDF).

The neutron source that is used for vessel fluence calculations should include spatial, temporal, and energy dependence. The temporal dependence of the flux should be determined from depletion calculations. The neutron source should be determined by using a combination of the power distribution, power level, and fuel management scheme. A best estimate approach may be used to determine the power distribution. The peripheral assemblies contribute heavily to the vessel fluence calculation and their radial power gradients should not be neglected.

Vessel fluence calculations can be performed using either deterministic or Monte Carlo methods. The NRC guidelines outline both of these methods, however this thesis focuses on Monte Carlo methods. The Monte Carlo method has a couple of advantages including: exact geometrical representation and use of continuous-energy cross sections. Geometry specification should be thoroughly checked or a pre-processor should be used due to the complexity of the general geometry input. The major drawback of Monte Carlo calculations is the significantly higher computational times for comparable accuracy to deterministic methods; a result of very few neutrons born in the core reaching the pressure vessel. Very large computational times are needed to get acceptably low relative errors. To counter this, variance reduction techniques can be applied. These methods include:

1. Neutron energy cutoff
2. Source biasing
3. Geometry splitting with Russian Roulette
4. Weight windows

Applying these variance reduction methods can greatly reduce statistical uncertainty and computational times. If any of these variance reduction techniques are used, extensive benchmarking and comparisons should be performed to ensure their accuracy.

This document also provides guidelines for comparing against benchmark measurements and calculations. For comparison to a simulation benchmark, calculations should be compared at the inner surface, T/4, and 3T/4 positions of the reactor pressure vessel. The validation should include comparisons of reaction rates, neutron fluence, and group fluxes at the location of interest. Methods for determining the vessel fluence should remain consistent with those used for determining the benchmark solution. This includes, cross sections, transport techniques, and transport parameters that are used. Differences between calculations and benchmarks should be within the combined uncertainty estimates. For use in 10 CFR 50, uncertainty of the fluence should be below 20% for determining radiation embrittlement effects.

This guide provides a great deal of information for performing pressure vessel neutron fluence calculations. A few points from this thesis are especially important to consider moving forward with

this thesis. One of the most important things to consider is the importance of peripheral assemblies in vessel fluence calculations. When performing homogenization, it will be essential to capture the physics in the peripheral assemblies to get accurate results. However, the same emphasis was not placed on assemblies towards the center of the core; which validates the idea of homogenizing these temperatures and densities. This thesis also validated the use of Monte Carlo methods for performing vessel fluence calculations.

Watts Bar Reactor Vessel Surveillance Program

The NRC requires utilities to maintain a reactor vessel material surveillance program. This program is intended to monitor neutron irradiation of the pressure vessel beltline and the impact on the material tensile properties[12]. As part of this program, at Watts Bar Unit 1, Capsule W was removed from the Watts Bar Unit 1 reactor vessel after 3.81 effective full-power years. The post-irradiation mechanical properties of this capsule were tested by BWX Technologies at their hot cell facility.

During the initial construction, a total of six surveillance capsules were inserted into the reactor pressure vessel of Watts Bar Unit 1[12]. The location of each capsule is shown in Fig. 1.1. Capsule W, used in this investigation, was constructed to contain identical materials to those around the beltline of the pressure vessel; including the submerged arc weld. The capsule included specimens for determining the Charpy impact and tensile properties of the irradiated sample. Dosimeter wires of pure copper, iron, nickel, aluminum and cobalt are included in the capsule. In addition, Np^{237} and U^{238} dosimeters are used to measure the fluence at specific neutron energy levels.

A number of investigations were performed with this surveillance capsule including[12]:

1. Visual examination and inventory
2. Thermal monitors
3. Charpy impact testing
4. Tensile testing
5. 1/2T compact tension and bend bar specimen tests

Based on visual examination and thermal monitors, it was determined that no discrepancies were found and the maximum temperature never exceeded 579°F[12]. Results from the Charpy impact testing were less limiting than the estimations provided in the regulatory guide and shows the predictions are conservative. As the neutron fluence increased, tensile testing showed that strength increased and ductility decreased. This is expected behavior from radiation embrittlement.

This analysis included an investigation of the neutron dosimetry using a state-of-the-art neutron transport calculation. This neutron transport calculation was performed following the guidelines

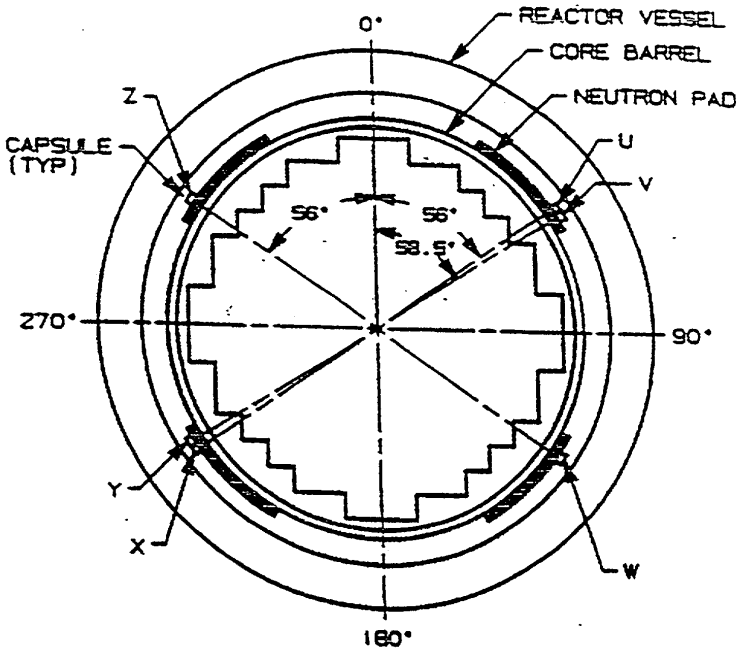

Figure 1.1 Arrangement of surveillance capsules in Watts Bar Unit 1 reactor vessel [12]

set forth by the Nuclear Regulatory Commission[1]. This calculation was performed using the deterministic code, Two-Dimensional Discrete Ordinates Radiation Transport (DORT)[14]. DORT utilized a 47-group ENDF/B-VI based cross section library. In accordance with guidelines, the absolute calculation is transported to the reactor vessel. A bias was found between the deterministic results and measured results. Since the calculated bias was within the allowable limit of 20%, calculated values are scaled by a factor of 1.162 to correct for the bias[12]. After correcting for the bias, uncertainties for the fluence at the vessel inner radius and 1/4T position were between 13-15%.

This thesis provided an overview of how vessel fluence calculations were performed in the past and are still conducted in the nuclear industry. Experimental measurements were the primary method for estimating pressure vessel embrittlement and other material changes. These experiments are difficult and limited by the number of capsules and their positions at the beginning of the plant life. Neutron transport approximations were limited to a multigroup deterministic solution with a number of assumptions for collapsing cross sections. Higher fidelity computational models such as Monte Carlo neutron transport can provide a more accurate evaluation of vessel fluence.

Monte Carlo Fluence

In 1996, Wagner et. al. investigated the use of Monte Carlo methods for pressure vessel fluence calculations[17]. This investigation utilized MCNP[7] and compared the results to the deterministic code DORT[14]. The Three Mile Island(TMI) unit 1 reactor was modeled for this problem. Wagner et. al. investigated the use of ex-vessel cavity dosimetry for measuring vessel irradiation, but recognized the numerous complications in performing these evaluations. Modeling ex-vessel dosimetry is particularly difficult due to strong attenuation through the pressure vessel and three-dimensional(3D) streaming through the cavity region. These modeling complications necessitated a more accurate method than conventional S_N transport calculations; thus Monte Carlo was chosen. Monte Carlo has the advantage of 3D geometrical modeling and continuous-energy cross sections.

Prior to this work, very few investigations had been performed using Monte Carlo for vessel fluence calculations and none calculated the neutron flux throughout the reactor system[17]. The expense of performing Monte Carlo simulations of such a large and complex system is extremely limiting; thus, S_N transport methods have been typically used. An increase in computer performance made this investigation possible in 1996, but even with newer computational power, a number of assumptions are made to make the problem practical. One such assumption that was made for this investigation is that source neutrons are only born in the peripheral two layers of assemblies. This assumption was made to increase the efficiency of the calculation and reduce memory usage. The TMI reactor geometry as modeled in MCNP is shown in Fig. 1.2. The MCNP model explicitly modeled all rectangular and cylindrical geometries, while DORT approximated rectangular geometries using jagged arcs. MCNP utilized a continuous energy library based on ENDF/B-V; while DORT used a 47-group cross section library based on ENDF/B-IV.

A number of variance reduction techniques are available in MCNP to improve the efficiency of the calculations. In this investigation, Wagner et. al. utilized energy cutoff, source biasing, weight windows, and exponential transformation[17]. Energy cutoff was used to "kill" any particle below 1 MeV and source biasing was used to produce neutrons with high energy moving towards the outside of the core. Weight window split described the spatial-energy importance and exponential transformation stretched the distance between collision in the desired direction. Particle splitting was not used for this investigation. Wagner et. al. also mention the potential benefit of using hybrid methods, utilizing adjoint solutions as an importance map for geometrical splitting.

In the reactor pressure vessel, MCNP predicted fluxes that were regularly 15% to 20% higher than those found using DORT[17]. These differences however, were largely attributed to the cross section group structures used in DORT and not to geometrical or dimensionality approximations. Multigroup MCNP analysis was performed and showed a 171-group structure had significantly better agreement to the continuous-energy MCNP than a 47-group structure. MCNP using the recommended cross sections, ENDF/B-V with Group T-2 iron data, came within 7% of all measured

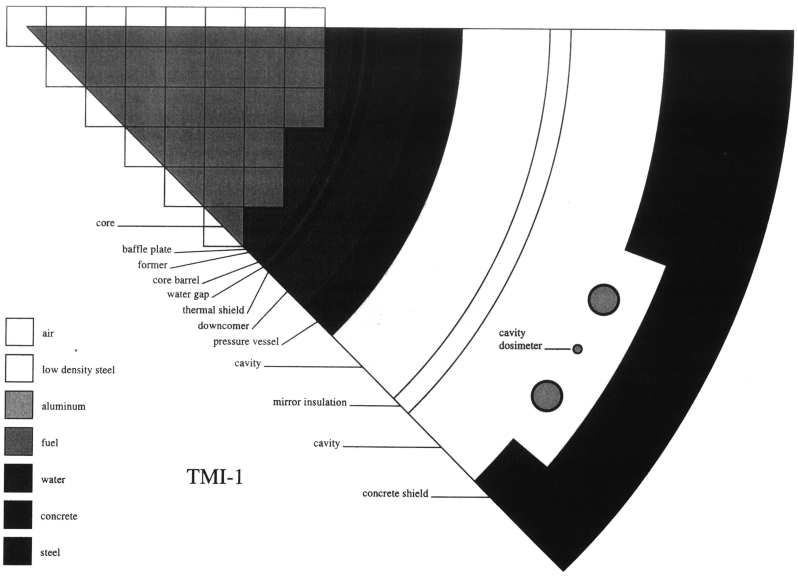

Figure 1.2 The TMI-1 reactor as modeled in MCNP[17]

reaction rates. The use of the adjoint function to generate weight windows was shown to dramatically reduce computational time, compared to generic weight window generation. The same relative difference could be achieved in roughly 1/4 of the time.

This investigation by Wagner et. al. provided a number of insights that are useful in this thesis. The assumption used for this study that particles born in the interior of the core are negligible for vessel fluence calculations, supports the idea of homogenizing temperatures and densities in the interior of the core. If neutrons that are born in the interior of the core can be assumed to be negligible; the reactor conditions on the interior of the core are less influential. This also supports explicitly modeling temperature and density in peripheral pincells.

Another finding from this study, relevant to this thesis is the benefit of using hybrid variance reduction techniques. In one of the first uses of a deterministic neutronics solvers for automated variance reduction, Wagner et. al. showed a factor of 4 computational efficiency increase over conventional methodology. Since this investigation, automated variance reduction method have been implemented in a number of codes; including Shift. One option in Shift, that is particularly relevant for vessel fluence calculations, is utilizing **C**onsistent **A**djoint-**D**riven **I**mportance **S**ampling (CADIS) to automate variance reduction; using the adjoint flux to generate weight windows[10] [13]. This functionality is essential for large, complex problems.

Code Overview

VERA

The **V**irtual **E**nvironment for **R**eactor **A**pplications (VERA) is the foundational code developed by the Consortium for Advanced Simulation of Light Water Reactors (CASL) [8]. VERA is intended to provide higher-fidelity results than industry standards by incorporating coupled physics models and modern computational science. One component of VERA is the VERA **C**ore **S**imulator (VERA-CS)[8].

VERA-CS is the collection of multiphysics codes that are used to model a reactor. Separate codes in VERA-CS are capable of neutron transport, depletion, thermal-hydraulics, and fuel performance calculations[8]. One of the most advantageous features of VERA-CS is the VERA common input. An additional benefit is that a single geometry input reduces errors from inconsistent geometry specifications between codes[9].

For this thesis, CTF, MPACT, and Shift were used within VERA-CS. These specific codes are discussed below.

CTF

CTF is the improved and modernized version of the **Co**olant **B**oiling in **R**od **A**rrays - Two Fluid (COBRA-TF) thermal-hydraulics code[15]. The code is maintained by CASL and North Carolina State University. CTF is a sub-channel, thermal-hydraulics code intended for light water reactor (LWR) core analysis. CTF utilizes a two-fluid approach, with three independent flow fields; fluid film, vapor, and liquid droplets[15]. These flow fields are modeled using three momentum, three mass, and two energy conservation equations. These equations can be solved on a 3D Cartesian mesh or with a sub-channel model. Interaction terms are used within CTF to link the conservation equations and all equations are solved simultaneously.

CTF is used withing VERA-CS as the primary thermal-hydraulic solver for modeling reactor heat transfer. CTF is coupled with MPACT to accurately model reactor conditions during normal and transient operation.

MPACT

The **M**ichigan **Pa**rallel **C**haracteristics based **T**ransport (MPACT) code is intended to perform high-fidelity LWR neutronics calculations using the Method of Characteristics (MOC)[2]. While the code is capable of using 3-D MOC, for full core simulations a 2D-1D MOC scheme is utilized. This 2D-1D method is performed by dividing the core into many planes and determining the MOC solution for each plane. The axial solution is then computed using a lower-order one-dimensional diffusion or P_3 approximation. Each of these axial divisions are between 5-10 cm thick. The 2D solution is

derived from the steady-state continuous form of the Boltzmann neutron transport equation given in Eq. 1.1[2].

$$\Omega \cdot \nabla \Psi(x,\Omega) + \Sigma_t \Psi(x,\Omega) = \frac{\Sigma_s}{4\pi} \int_{4\pi} \Psi(x,\Omega') d\Omega' + \frac{\nu \Sigma_f}{4\pi k} \int_{4\pi} \Psi(x,\Omega') d\Omega' \tag{1.1}$$

What sets MOC apart from other discrete ordinates methods for solving the neutron transport equation is how the problem space is discretized. The problem is discretized by choosing a set of rays that represent the flight paths of the neutrons through the problem domain[2]. Any set of rays can be selected as long as the intersection between the ray and the spacial region boundaries can be determined. These characteristic rays are demonstrated in Fig. 1.3.

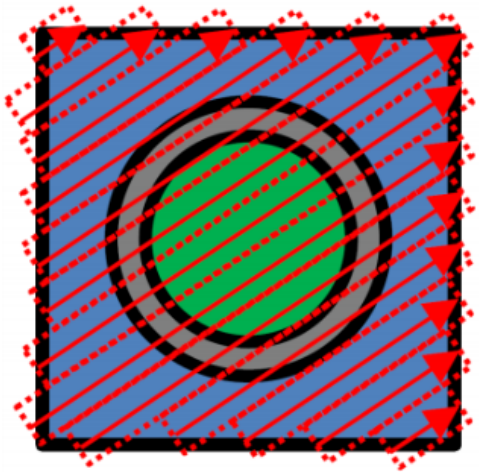

Figure 1.3 Characteristic rays through a pincell[2]

In this investigation, MPACT was used within the VERA-CS environment coupled with CTF and Shift. From the coupled MPACT/CTF calculation, shown in Fig. 1.4, the fission source, fuel temperature, clad temperature, moderator temperature, and moderator density are passed to Shift.

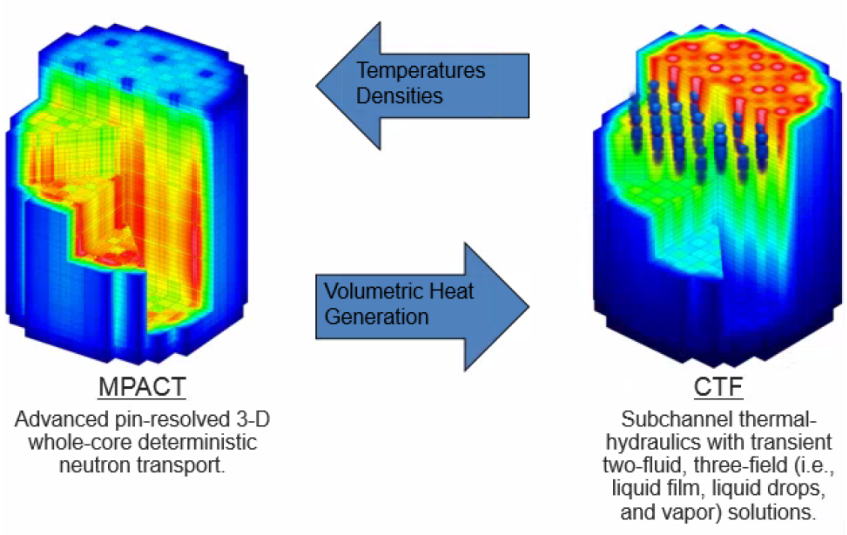

Figure 1.4 MPACT and CTF coupling scheme[4]

VERAShift

The VERAShift package couples VERA-CS and Shift to perform benchmarking and excore calculations tallies.

Shift is a continuous-energy Monte Carlo radiation transport code developed at Oak Ridge National Laboratory and is included in the SCALE code package[10]. Shift has been developed for fast and accurate transport calculations by utilizing massively parallel computations. Shift scales well on high performance architectures and has been optimized for running radiation transport calculations on current and near future computing architectures. Shift has multiple geometry configurations that can be used; including a general specification that is used in the VERAShift coupling.

Shift utilizes spatially decomposed, energy-binned weight windows to perform variance reduction[10]. These weight windows can be implemented as an importance map from an adjoint Denovo calculation. Both Shift and Denovo exist in Exnihilo, a radiation transport code suite[6]. Along with the weight windows, Shift also implements a biased source that ensures consistency with the weight windows and source definition. During the biased source construction, Shift calculates the estimated response, shown in Eq. 1.2, that is used for renormalizing the weight windows. The CADIS methodology is utilized to automate this process[13].

$$R = \int\int q(\mathbf{r},E)\phi(\mathbf{r},E)dE\,dV = \int\int \frac{q(\mathbf{r},E)}{w(\mathbf{r},E)}dE\,dV \tag{1.2}$$

VERAShift can automate excore simulations for multiple state-points in a single run of the

code[11]. For default vessel fluence calculations, very little user input is required. VERAShift includes the capability to insert a detailed core model; including all isotopes and temperatures, generated in VERA-CS. While VERAShift can run in eigenvalue mode, a fixed source forward mode has been developed to perform excore simulations; using CADIS for variance reduction.

VERAShift employs a one-way coupling scheme to transfer temperatures, densities, isotopics, and the fission source from MPACT-CTF to Shift[11]. For each state-point, this information is used by Shift to automatically generate a detailed geometric core model for each state-point. A simple description of the transfer algorithm is shown in Alg. 1. Shift and MPACT run on separate processor domains; the MPACT-CTF calculation must finish a given state before beginning the Shift calculation for that state. However, the MPACT calculation for the subsequent state-point can begin while the Shift calculation is performed. The **D**ata **T**ransfer **K**it(DTK) is used to transfer the fission source, temperatures, densities, and isotopics from MPACT to Shift[16].

```
1  Parse MPACT-CTF and Shift input;
2  Setup MPI communicators;
3  Construct model evaluators;
4  Setup MPACT-CTF to Shift transfer;
5  for each state do
6      if processor running MPACT-CTF then
7          Run a single MPACT-CTF state-point calculation or depletion step calculation;
8          Pass temperatures, densities, isotopics, fission source to Shift;
9          Continue to next state;
10     else if processor running Shift then
11         Receive temperatures, densities, isotopics, and fission source from MPACT-CTF;
12         while stop_criteria do
13             Run forward or CADIS Shift and tally flux in vessel;
           end
   end
```

Algorithm 1: Simple VERAShift Algorithm[11]

The input for VERAShift is specified as a common VERAIn input file and parsed for use by individual codes automatically[9]. General information such as: geometry, materials, and reactor conditions are shared between all codes in VERA-CS. The SHIFT block is used for setting parameters such as: CADIS options, number of particles, and tally specifications [11]. The majority of results for VERAShift are output to Hierarchical Data Format 5 (HDF5) including: tallies, pin powers, memory usage, mesh statistics, and adjoint flux[5]. All state-points are output to the same file in separate datasets.

CHAPTER

2

CORE APPROXIMATION TECHNIQUES

Temperature and Density Homogenization Methods

The objective of this thesis is to investigate core approximation techniques. Specifically, this thesis investigates the impact of various temperature and density homogenizations in a reactor core on vessel fluence calculations. These homogenizations are intended to decrease the memory usage in VERAShift and simplify the problem. These memory reductions are two-fold; reducing the number of cross-section libraries used by reducing the number of unique temperatures, and reducing the number of unique pincells by only making a single unique pincell for each homogenization location. The methods for memory savings will be discussed further with semi-unique pincells.

Assembly-Averaged Homogenization

The first homogenization method considered is a simple assembly-averaged, homogenization of temperature and density. This homogenization was selected due to its simplicity and prior use for core calculations.

This homogenization consists of volume average temperature and density homogenizations for each assembly in the core. In the case of quarter symmetry, the volumes used in homogenization are adjusted by a factor of $1/2$ or $1/4$ for half or quarter pincells respectively. An example of assembly-averaged homogenization is shown in Fig. 2.1.

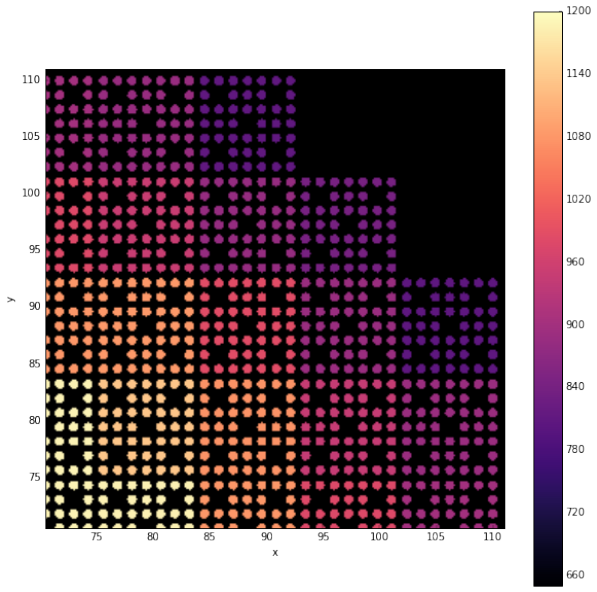

Figure 2.1 Assembly-average homogenization: fuel temperatures(K)

Ring Averaged Homogenization

The second homogenization technique selected is ring averaged temperature and density homogenization. This homogenization was selected to take advantage of radial symmetry in nuclear reactors.

This homogenization consists of volume average temperature and density homogenizations in radial rings throughout the core. In the case of symmetry, the volumes used in homogenization are adjusted by a factor of $1/2$ or $1/4$ for half or quarter pincells, respectively. The ring based homogenization is dictated by the distance from the center of the core. There are two options for ring homogenization: assembly or pin based. For assembly ring homogenization, the distance to the center of the core is determined from the center of the containing assembly. For pin ring homogenization, the distance to the center of the core is determined from the center of the containing pin. An example of ring-averaged homogenization is shown in Fig. 2.2. Thin white lines are used to show boundaries between rings for pin rings.

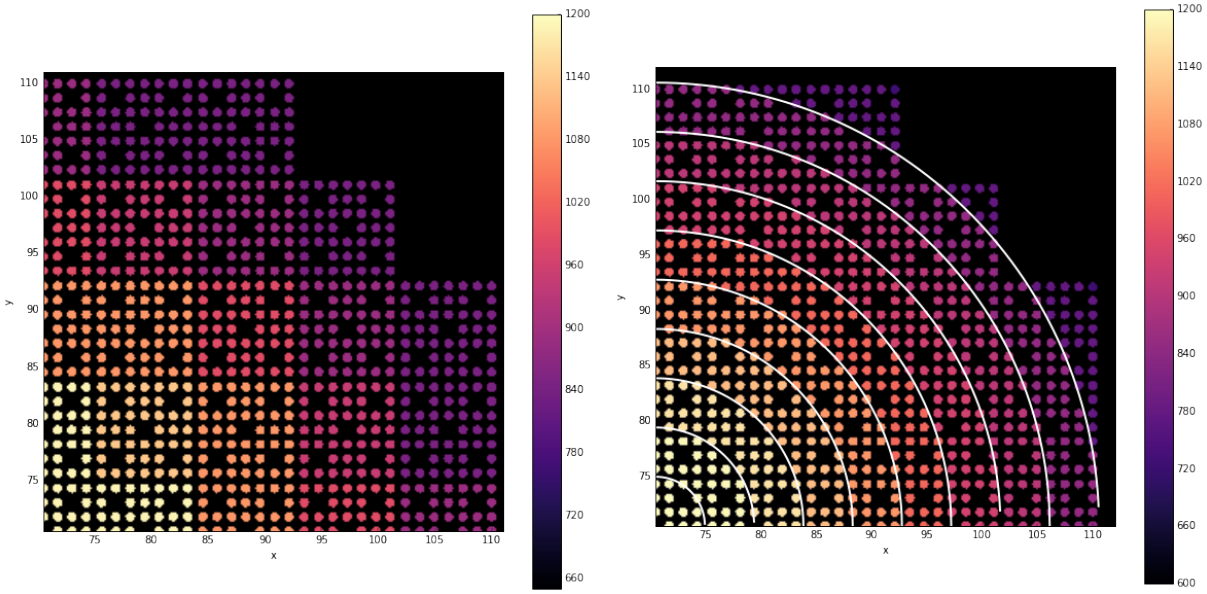

(a) Assembly-ring averaged

(b) Pin-ring averaged

Figure 2.2 Ring averaged homogenizations: fuel temperature(K)

Explicit Peripheral Pins

As mentioned in [1] and [17], the conditions on the periphery of the reactor core are extremely influential for vessel fluence and excore calculations. Due to the importance of outer pins and assemblies, it is essential to explicitly model the physics in the outer assemblies of the core. The explicit peripheral pins option for homogenization was implemented in Shift to avoid homogenizing temperatures and densities for pincells on the periphery of the reactor core. Explicit peripheral pins can be used with either ring or assembly homogenization schemes. The explicit peripheral pins are user-specified by inputting a radial distance from the center of the core. Outside of this ring, temperature and densities are modeled explicitly for each pin location. Fig. 2.3 demonstrates this homogenization method for assembly and ring homogenizations. Thick white lines are used to show the boundary for explicit peripheral pincells. Thin white lines show ring boundaries.

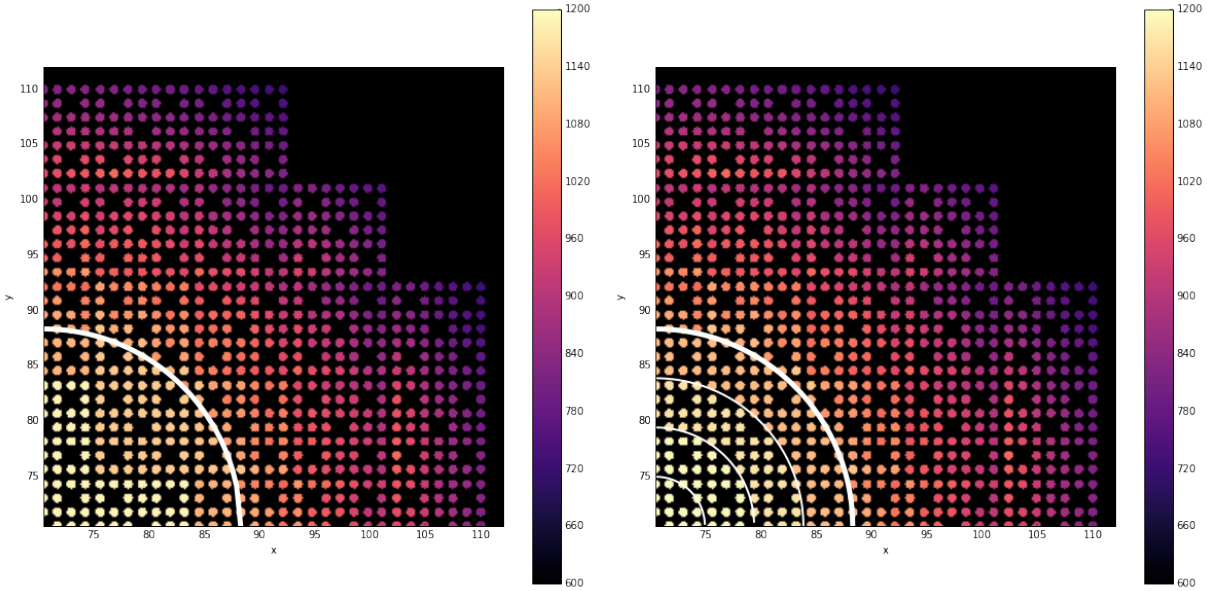

(a) Assembly-ring averaged with explicit peripheral pins **(b)** Pin-ring averaged with explicit peripheral pins

Figure 2.3 Explicit peripheral pins homogenization option: fuel temperature(K)

Pincell Classifications

Currently there are two options in VERAShift for modeling the geometrical and material specifications. Users have the option of using unique or nonunique pincells. In order to alleviate memory restrictions, semi-unique pincells were introduced for homogenization.

Unique Pincells

One option in VERAShift is unique pincells. If unique pincells are selected, each pincell in the core is uniquely defined in the core metadata. Unique pincells allow for a higher level of detail in the reactor core model. Geometric and material properties are saved for each pincell; allowing them to be individually altered. This option enables temperature, density, and isotopics transfer from the VERA-CS calculation to Shift. Unique pincells require substantially more memory usage compared to nonunique pincells. This becomes extremely limiting for modeling full reactor models. Fig. 2.4 shows the pincell id for each position in a simple 3x3 example core. Each unique color represents a different assembly. The figure shows that each pincell has a unique specification.

Figure 2.4 Unique pincell specification: pincell ID

Nonunique Pincells

Currently the only alternative in VERAShift to fully unique pincells is nonunique pincells. When using nonunique pincells, temperature and density variations throughout the core are ignored and all materials are set to the initial properties provided in the VERA input. The fission source distribution is the only information transferred from VERA-CS. While nonunique pincells use significantly less memory than unique pincells, the lack of detail in the model can lead to much less accurate results. Fig. 2.5 shows the pincell id for each position in a simple 3x3 example core. Each unique color represents a different assembly. A single unique pincell is created and replicated throughout the core.

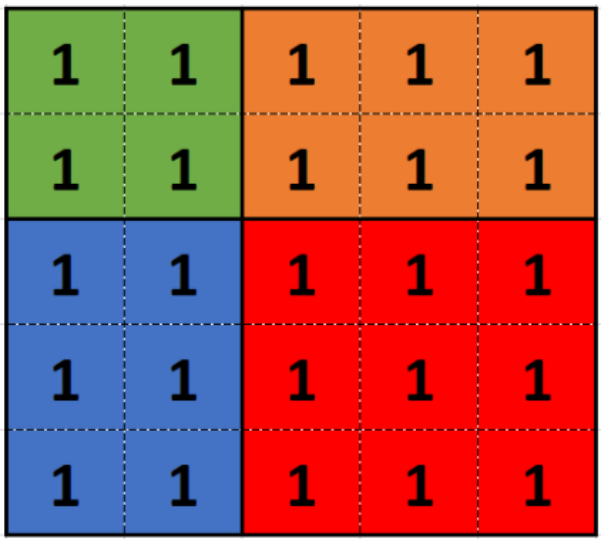

Figure 2.5 Nonunique pincell specification: pincell ID

Semi-Unique Pincells

Semi-unique pincells were introduced as part of this thesis for use in the temperature and density homogenization investigations. Semi-unique pincells are intended to bridge the gap between nonunique and all unique pincell configurations. With this specification, each "homogenization location" is uniquely specified in the core metadata. For instance, with ring homogenization, each radial ring would be represented by at least one uniquely defined pincell. This allows for temperature and density transfer from the VERA-CS calculation to Shift. In addition to temperature and density detail for each "homogenization location", semi-unique pincells also use significantly less memory than fully unique pincells. Fig. 2.6 shows the pincell id for each position in a simple 3x3 example core. Each unique color represents a different assembly. For this example, we are considering an assembly homogenization. A unique pincell is created in each assembly and replicated throughout that assembly.

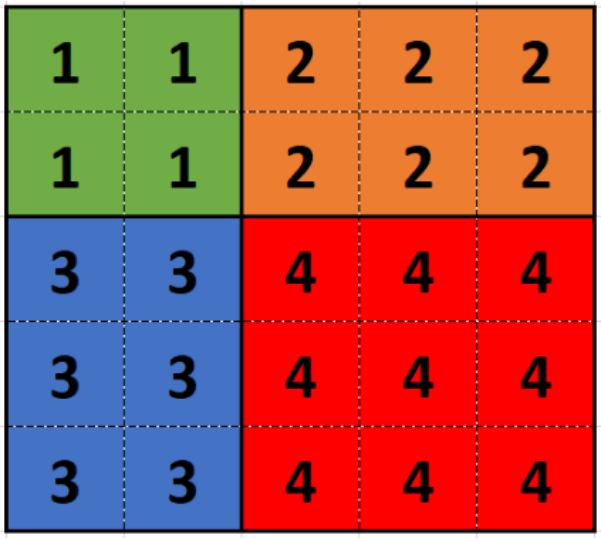

Figure 2.6 Semi-unique, assembly-homogenized, pincell specification: pincell ID

CHAPTER

3

PROBLEM DESCRIPTION

AMA Problem 7

In order to test the homogenization methods, explained in Chapter 2, we used CASL Core Physics Benchmark Progression problem 7[3]. Problem 7 is intended to demonstrate a code's performance in modeling an operating reactor in full detail. Specifically, problem 7 models the hot full power, beginning of cycle, 3D, Watts Bar cycle 1 core. For our analysis, we considered the full problem 7 specification as well as a mini core configuration, developed under CASL for MPACT testing. The two configurations share a number of similarities. Table 3.1 shows the geometry specifications that are shared between the two configurations.

In addition to sharing a number of geometry specifications, the two configurations also share material compositions. The material specifications are given in Appendix A.

Table 3.1 AMA problem 7 shared geometry specifications

Parameter	Value
Pin Radius	0.4096 cm
Clad Inner Radius	0.418 cm
Clad Outer Radius	0.475 cm
Pin Pitch	1.26 cm
GT Inner Radius	0.561 cm
GT Outer Radius	0.602 cm
Inlet Coolant Temperature	565 K
Reactor Pressure	2250 psi

Mini-Core Model

The first configuration that is considered is a simple 9x9 reactor core. Each assembly in the core is a 7x7, scaled down, 17x17 Westinghouse, PWR fuel assembly. This model was selected to mimic typical reactor conditions. Due to it's smaller size, this model requires significantly less computational resources than a full reactor core. Due to symmetry, this core can be modeled using quarter core symmetry. The geometry specifications for this core are shown in Table 3.2.

The 7x7 pin lattice contains four guide tubes and an instrument channel in the center of the assembly. The remaining positions in the assembly contain fuel. The fuel pin lattice layout is shown in Fig. 3.1.

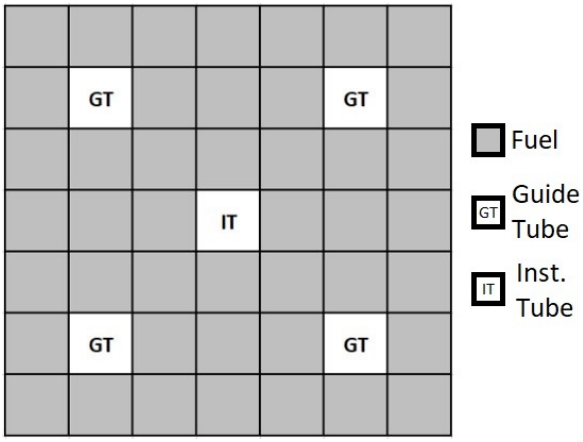

Figure 3.1 Mini-core assembly layout[3]

Table 3.2 AMA problem 7 mini-core specifications

Parameter	**Value**
Fuel Height	209.16 cm
Core Height	249.737 cm
Pin Lattice	7x7
Assembly Lattice	9x9
Assembly Pitch	8.9 cm
Number of Axial Regions	28
Rated Power	88.3333 MW
Rated Flow Rate	5.0865 Mlbs/hr
Barrel Inner Radius	60.0 cm
Barrel Outer Radius	64.0 cm
Vessel Liner Inner Radius	82.0 cm
Vessel Inner Radius	82.5 cm
Vessel Outer Radius	100.5 cm

The guide tubes in Fig. 3.1 can be filled with Pyrex, a burnable poison, control rods, or simply contain moderator. The number of Pyrex rods and fuel enrichment vary throughout the core. The assembly lattice indicating fuel enrichment and number of Pyrex rods are shown in Fig. 3.2.

Fig. 3.2 shows the fuel enrichment in each assembly. Enrichments are consistent across an assembly. Enrichments vary from 2.1% to 3.1% with the highest enrichments on the periphery of the core. A 2D slice of this model is shown in Fig. 3.3.

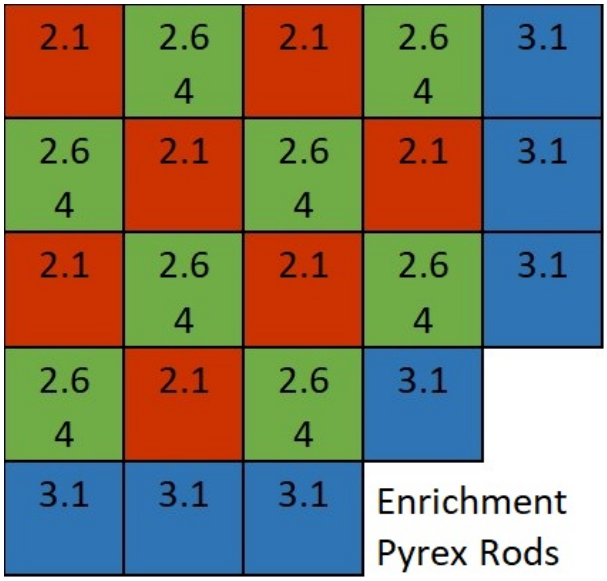

Figure 3.2 Mini-core enrichment layout[3]

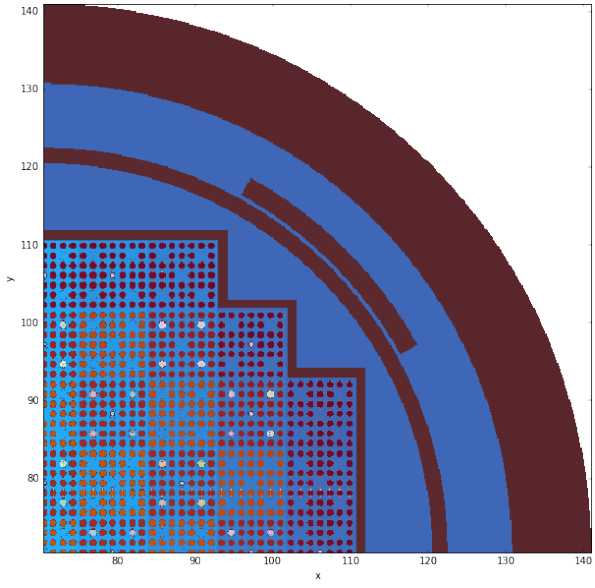

Figure 3.3 Mini-core geometry

Full Core Model

The other configuration that is considered is a complex 15x15 reactor core. Each assembly in the core is a 17x17 Westinghouse PWR fuel assembly. This model was selected to mimic typical reactor conditions during normal operations. Due to it's large size and complexity, the computational costs of this model are extremely limiting. Thanks to symmetry, this core can be modeled using quarter core symmetry. The geometry specifications for this core are shown in Table 3.3.

Table 3.3 AMA problem 7 quarter full-core specifications

Parameter	**Value**
Fuel Height	365.76 cm
Core Height	285.10 cm
Pin Lattice	17x17
Assembly Lattice	15x15
Assembly Pitch	21.6 cm
Number of Axial Regions	49
Rated Power	3411 MW
Rated Flow Rate	131.68 Mlbs/hr
Barrel Inner Radius	187.96 cm
Barrel Outer Radius	193.68 cm
Vessel Liner Inner Radius	219.15 cm
Vessel Inner Radius	219.71 cm
Vessel Outer Radius	241.70 cm

The 17x17 pin lattice contains four guide tubes and an instrument channel in the center of the assembly. The remaining positions in the assembly contain fuel. The fuel pin lattice layout is shown in Fig. B.12.

The guide tubes in Fig. B.12 can be filled with Pyrex, a burnable poison, control rods, or simply contain moderator. The number of Pyrex rods and fuel enrichment vary throughout the core. The assembly lattice indicating fuel enrichment and number of Pyrex rods are shown in Fig. 3.5.

Fig. 3.5 shows the fuel enrichment in each assembly. Enrichments are consistent across an assembly. Enrichments vary from 2.1% to 3.1% with the highest enrichments on the periphery of the core. A 2D slice of this model is shown in Fig. 3.6.

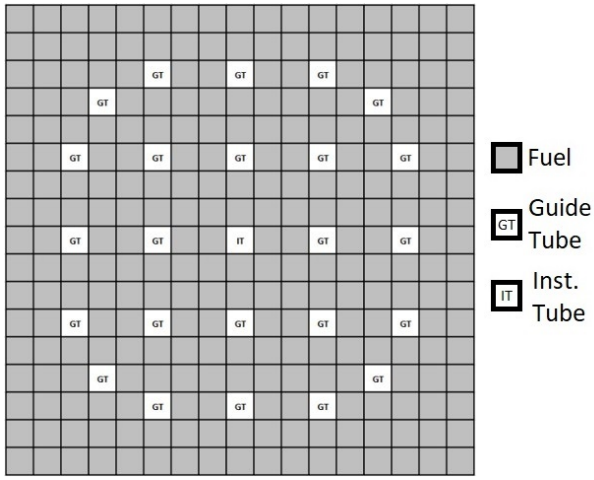

Figure 3.4 AMA problem 7 quarter full-core assembly layout[3]

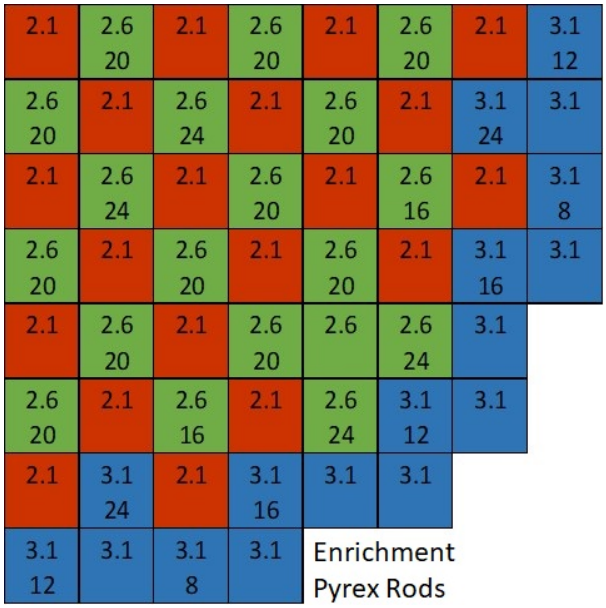

Figure 3.5 AMA problem 7 quarter full-core enrichment and poison rod layout[3]

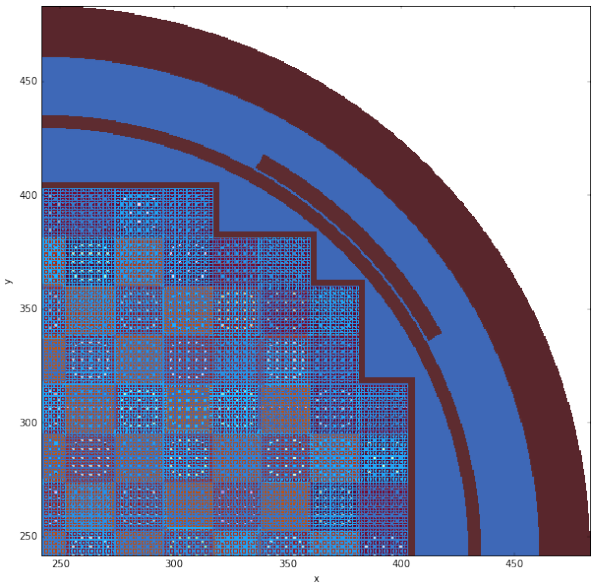

Figure 3.6 AMA problem 7 quarter full-core geometry

VERA Problem Parameters

This section covers the parameters that were used within VERA to perform vessel fluence calculations.

MPACT-CTF

A coupled calculation was performed between MPACT and CTF to first determine the temperature, density, and fission source distributions. The parameters used in this study for the mini-core are shown in Table 3.4. Default values were used for every parameter in the quarter full-core model.

Table 3.4 MPACT-CTF problem specifications

Parameter	**Value (mini/full)**
VERA	
Power	88.3333/3411
Flowrate	5.0865/131.68
Symmetry	qtr
Xenon	equil
Feedback	on
MPACT	
Ray Spacing	0.08
Shield Ray Spacing	0.08
Azimuthal Angles	16
Polar Angles	2
Resonance Up-Scatter	false
k Tolerance	$1e-5$
Flux Tolerance	$5e-5$
CTF	
β	0.005
Max Iterations	10000
ϵ	0.00001

Shift

Shift is run within VERAShift and shares all geometry material specifications defined in the general blocks within VERA. Parameters specific to Shift are defined in the [SHIFT] block of the VERA common input[11]. Most of the parameters used in this investigation were the same for both core configurations. The parameters used in this study are shown in Table 3.5. For parameters that vary between configurations, both values are indicated.

Table 3.5 Shift problem specifications

Parameter	**Value (mini/full)**
Problem Mode	cadis
Number of Particles	$10^8/10^9$
Transport	Continuous Energy
Hybrid DB	
Pn Order	0
Adjoint	true
Equation Set	sc
mesh	1
Dimension	3
Number of Blocks (i/j)	5
XS Library	v7-56
Number of Groups	8
Group Bounds	$6.0653E+06$ $3.6788E+06$ $2.3457E+06$ $1.6530E+06$ $8.2085E+05$ $2.4176E+04$ $1.0130E+02$ $1.0000E-05$
Cell Homogenize	true
Max ΔZ	5.0
Upscatter Subspace Size	200
Tally DB	
Neutron Bounds	$2.0e7$ $1.0e6$
Number of Theta Divisions	64/128
Number of Axial Divisions	10

Homogenization Comparison

In order to test the impact of these core approximations, a number of comparisons were performed. These comparisons were designed to investigate: the accuracy of semi-unique pincells, the impact of various homogenizations on vessel fluence, and the performance improvements from homogenization. For the mini-core model, results were compared to a fully explicit temperature and density model. The quarter full-core results were compared to the most accurate, achievable, homogenization. The specific comparisons investigated in this project for the mini-core configuration are listed in Table 3.6. The homogenizations considered for the quarter full-core model are listed in Table 3.7. In addition to these descriptions, the fuel temperature profile is presented for each homogenization in Appendix B. In these temperature profiles, thick white lines show the boundary, beyond which, explicit peripheral pincells are used and thin white lines represent pin-ring boundaries.

A number of investigations were performed in each of the cases presented in Table 3.6 and Table 3.7. For each case, relative differences in pressure vessel fluence were calculated and superimposed on the reactor geometry at the core midplane. In addition, diagnostics over all tally bins in the pressure vessel are tabulated including: maximum, minimum, absolute average, and average differences. From the mini-core investigation, the most accurate homogenization is selected for use in the realistic core configuration.

Table 3.6 Mini-core homogenization comparison cases

Name	Description
Unique vs. Semi-Unique	
uvs_full	Explicit temperature modeling: unique vs semi-unique
uvs_assem	Assembly-averaged homogenization. Shown in Fig. B.1: unique vs semi-unique
uvs_exassem	Assembly-averaged homogenization with explicit peripheral pins. Shown in Fig. B.2: unique vs semi-unique
uvs_ex1ring	Single temperature ring and explicit peripheral pins. Shown in Fig. B.10: unique vs semi-unique
uvs_pinring	Evenly distributed temperature rings. Shown in Fig. B.6: unique vs semi-unique
uvs_assemring	Assembly-averaged ring homogenization. Shown in Fig. B.5: unique vs semi-unique
Semi-Unique vs. Semi-Unique Homogenization Comparison	
svs_assem	Assembly-averaged homogenization. Shown in Fig. B.1
svs_exassem	Assembly-averaged homogenization with explicit peripheral pins. Shown in Fig. B.2
svs_exassem2	Assembly-averaged homogenization with more explicit peripheral pins. Shown in Fig. B.3
svs_1ring	Single temperature ring. Shown in Fig. B.4
svs_ex1ring	Single temperature ring with explicit peripheral pins. Shown in Fig. B.10
svs_assemring	Assembly-ring averaged homogenization. Shown in Fig. B.1
svs_pinring	Evenly distributed temperature rings. Shown in Fig. B.6
svs_pinring2	Thicker evenly distributed temperature rings. Shown in Fig. B.7
svs_multiring	Multiple temperature pin-rings of varying thickness. Shown in Fig. B.11
svs_expinring	Evenly distributed temperature rings with explicit peripheral pins. Shown in Fig. B.6
svs_expinring2	Evenly distributed temperature rings with more explicit peripheral pins. Shown in Fig. B.7
Enrichment Investigation	
enrich_assem	svs_assem with uniform enrichment
enrich_pinring	svs_pinring with uniform enrichment
enrich_expinring	svs_expinring with uniform enrichment
enrich_expinring2	svs_expinring2 with uniform enrichment

Table 3.7 Quarter-core homogenizations

Name	**Description**
Assembly	Assembly-averaged temperature and density homogenization. Shown in Fig. B.12
One Ring	Single temperature and density ring homogenization. Shown in Fig. B.13
Assembly Ring	Assembly-averaged temperature and density homogenization. Shown in Fig. B.14
Coarse Ring	Coarse temperature and density pin ring homogenization. Shown in Fig. B.15
Medium Ring	Medium thickness temperature and density pin-ring homogenization. Shown in Fig. B.16
Fine Ring	Fine temperature and density pin-ring homogenization. Shown in Fig. B.17

CHAPTER

4

HOMOGENIZATION RESULTS

In this thesis, we evaluated the use of core approximations, namely temperature and density homogenization and their impact on vessel fluence calculations. As part of this investigation, we validated the use of semi-unique pincells, determined the impact of various homogenizations, and studied the performance enhancements from these approximations.

Mini-Core

First, we considered the benchmark solution utilized for this analysis. This solution was generated using fully explicit temperature and density modeling throughout the core. A 2D, radial, depiction of the reactor pressure vessel neutron fluence, at the reactor midplane, is shown in Fig. 4.1. Fig. 4.2 shows the axial pressure vessel neutron fluence radially through the pressure vessel; taken at $\theta = \frac{\pi}{2}$.

As a Monte Carlo calculation, all fluence tallies have an associated uncertainty. This uncertainty is important for determining the accuracy of the results; especially when comparing to other results. Fig. 4.3 shows the relative standard deviation, calculated by Eq. 4.1, of each tally presented in Fig. 4.1. All of the uncertainties are below 2%.

$$\sigma_{rel} = \frac{\sqrt{\sigma_{abs}^2}}{\Phi} \tag{4.1}$$

As a consideration for the stochastic nature of Monte Carlo calculations, we began by performing

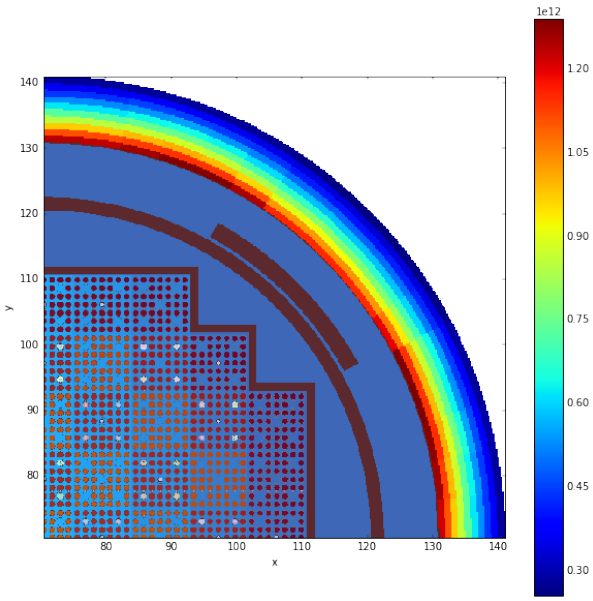

Figure 4.1 Mini-core radial neutron fluence (n/cm^2)

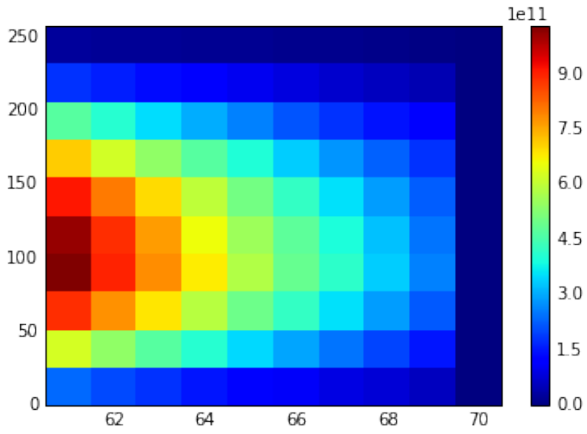

Figure 4.2 Mini-core axial neutron fluence (n/cm^2)

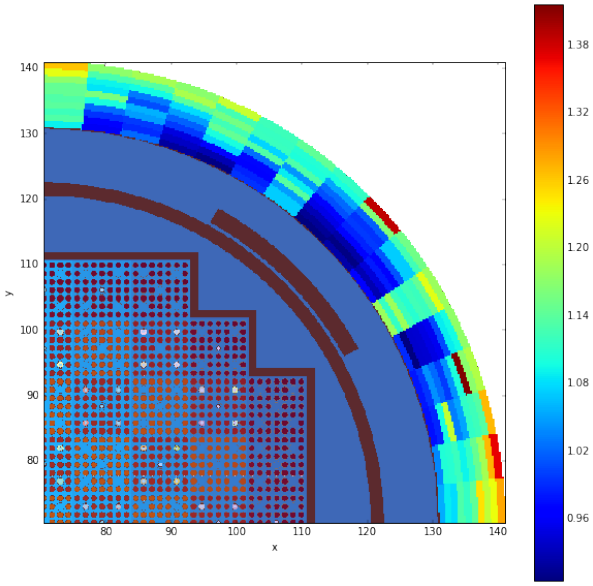

Figure 4.3 Mini-core pressure vessel neutron fluence uncertainty (%)

a fully unique, vessel fluence calculation with explicit temperature and density modeling; with two different random number seeds. This study provided us a baseline of the innate uncertainty in our calculations. Fig. 4.4 shows the relative differences in the neutron fluence between the same case using two different random number seeds.

This diagram was created from a 2D slice at the midplane of the reactor. The majority of differences were around or below 3% with higher uncertainties in a couple of bins. These differences mean little on their own, but provide a tool for determining the significance of differences when investigating homogenizations. To get a more complete picture of the differences in this case, some diagnostics are shown in Table 4.1.

Table 4.1 Stochastic comparison diagnostics

Measure	**Value(%)**
Maximum Difference	48.09
Minimum Difference	-20.79
Absolute Average Difference	1.42
Average Difference	-0.269

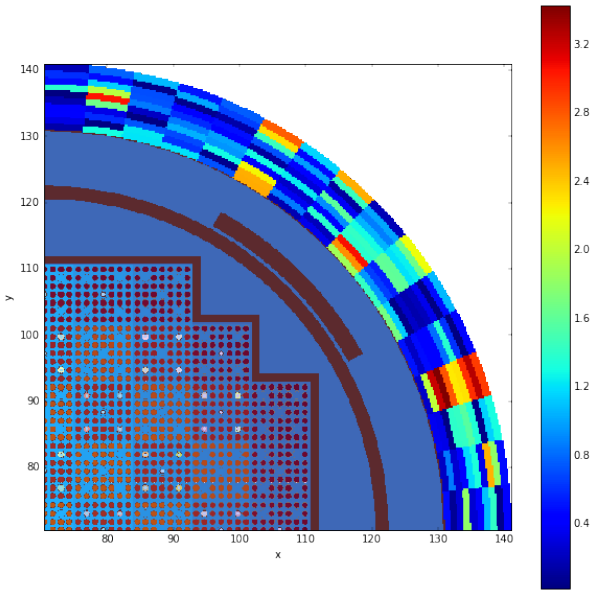

Figure 4.4 Stochastic relative differences (%)

As shown in Table 4.1 the maximum, minimum, absolute average, and average differences, over all axial levels, were 48.09%, -20.79%, 1.42%, and -0.269%, respectively. The differences were close to the expected values based on the uncertainties shown in Fig. 4.3. The absolute average differences between the cases were well within 2σ.

Another important consideration for this investigation is how each homogenization performs compared to the nonunique pincell configuration. Prior to this work, nonunique pincells were the only alternative to fully explicit temperature and density transfer using unique pincells. Nonunique pincells represents a core approximation with no temperature, density or isotopics transfer. The relative differences for this case are shown in Fig. 4.5.

For this case, the maximum, minimum, absolute average, and average differences, over all axial levels, were 27.09%, -19.05%, 2.13%, and -1.78%, respectively. While none of the individual differences were particularly large, it is clear from the average differences that the nonunique vessel fluence is significantly different than the explicit temperature and density model. Additionally, the vessel fluence calculated using nonunique pincells is shifted lower as evidenced by the absolute average difference. This means the nonunique solution is not only inaccurate, but also non-conservative.

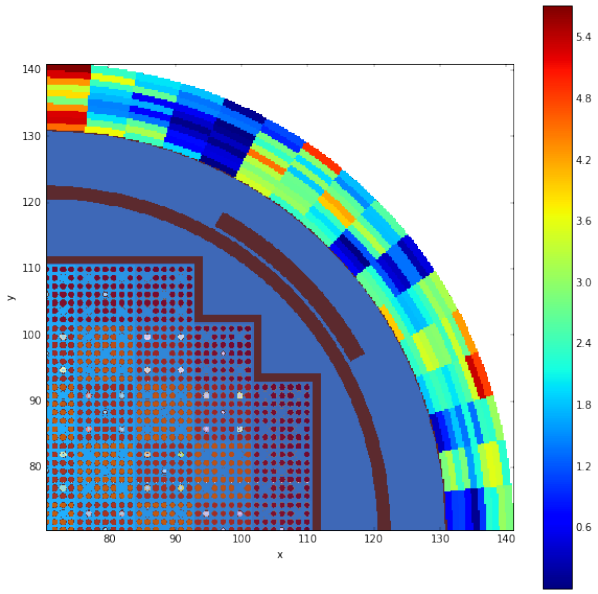

Figure 4.5 Nonunique pincell configuration relative differences(%)

Unique vs. Semiunique

Before benchmarking different homogenizations, it is important to determine the accuracy of the semi-unique pincells. This is important moving forward because all homogenization comparisons were performed using semi-unique pincells. In order to do this, the vessel fluence is compared for a variety of homogenization methods between unique and semi-unique pincells. The first case considered was fully explicit temperature and density modeling. This was accomplished using no homogenization for unique pincells and explicit peripheral pincells throughout the core for semi-unique pincells. The relative differences for this case are shown in Fig. 4.6.

For this case, the maximum, minimum, absolute average, and average differences were 33.76%, -19.64%, 1.34%, and -0.374%, respectively. All of these diagnostics, with the exception of average, showed a closer agreement than the baseline results shown in Table 4.1. Overall, it appears the semi-unique pincells performed well for a fully explicit temperature and density model. In addition to comparing the explicit temperature model, we also compared vessel fluence tallies for various homogenizations types. The first homogenization considered, was a simple assembly-averaged temperature and density homogenization. The relative differences for this case are shown in Fig. 4.7.

Similarly to Fig. 4.6, the relative differences appear to be randomly distributed with most differences at or below 2%. The maximum, minimum, absolute average, and average differences were 33.02%, −37.66%, 1.27%, and −0.073%, respectively. It appears that semi-unique pincells accurately modeled the assembly-averaged homogenization case. The majority of plots of the relative difference, for other homogenizations, look similar to those shown in Fig. 4.6 and Fig. 4.7 with the

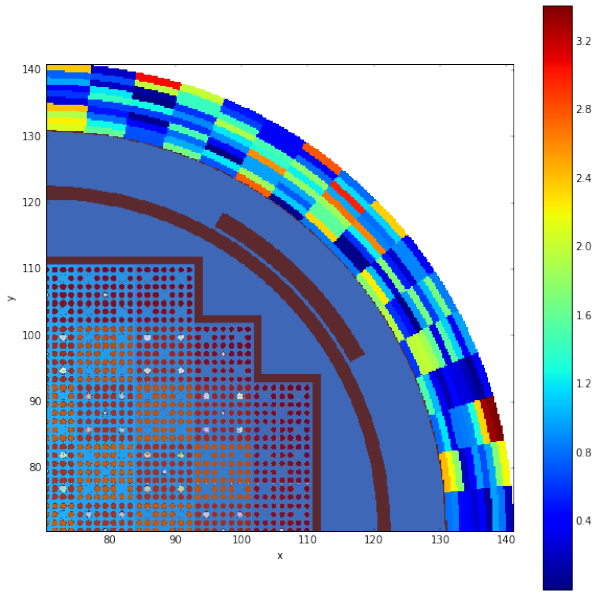

Figure 4.6 Explicit temperature and density model relative differences (%)

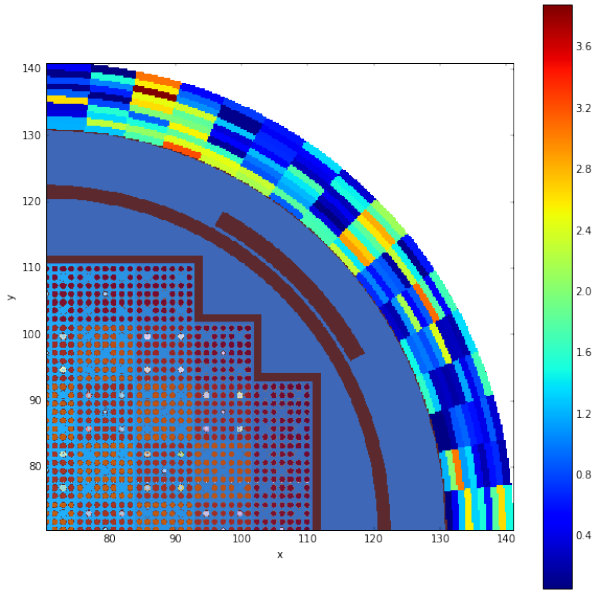

Figure 4.7 Assembly-averaged homogenization relative differences (%)

exception of the assembly-ring averaged homogenization case. The relative differences for this case are shown in Fig. 4.8.

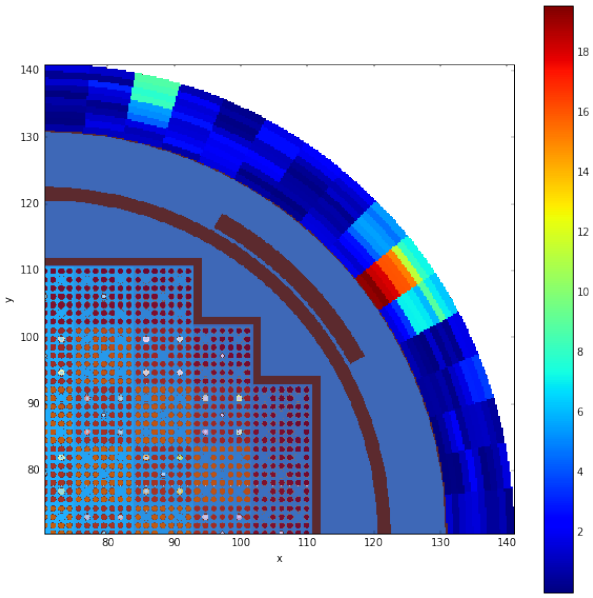

Figure 4.8 Assembly-ring homogenization relative differences (%)

Fig. 4.8 shows the relative differences between the vessel fluence for assembly-ring homogenizations using unique and semi-unique pincells. The differences in this case were higher than any of the other cases. The maximum, minimum, absolute average, and average differences were 82.95%, -19.59%, 1.62%, and -0.233%, respectively. While these differences could have been random, a result of the Monte Carlo method, they are higher than any other comparison and are considered when benchmarking the individual homogenizations.

The remaining difference plots are shown in Appendix C.1. All of these results look similar to Fig. 4.6 and Fig. 4.7. Diagnostics for these calculations are shown in Table 4.2.

Overall, the results listed in Table 4.2 were inline with those shown in Table 4.1. All of the absolute average differences were lower than the unique to unique baseline solution. This shows that the differences could be explained by the stochastic nature of the calculations.

The results of this investigation show that the semi-unique pincells are correctly modeling the reactor physics for explicit and homogenized temperature and density models. The one area of concern occurred in the assembly-ring homogenization case. In this case one azimuthal location had large differences when compared to the unique pincells solution. While these differences could have been caused by random discrepancies, the differences were higher than other cases.

Table 4.2 Unique vs. Semi-Unique

Case	Maximum	Minimum	Average	Absolute Average
uvs_exassem	33.63	-22.32	-0.010	1.37
uvs_ex1ring	58.63	-19.68	-0.236	1.33
uvs_1ring	35.03	-28.85	-0.446	1.36
uvs_pinring	73.80	-34.55	-0.289	1.25

Homogenization Analysis

In order to determine the accuracy of various homogenizations, a number of cases using different homogenizations were compared to an explicit temperature and density model. This evaluation was performed using semi-unique pincells. The first case that was considered was a simple assembly-averaged homogenization. The relative differences in vessel fluence, taken at the core midplane, for this case are shown in Fig. 4.9.

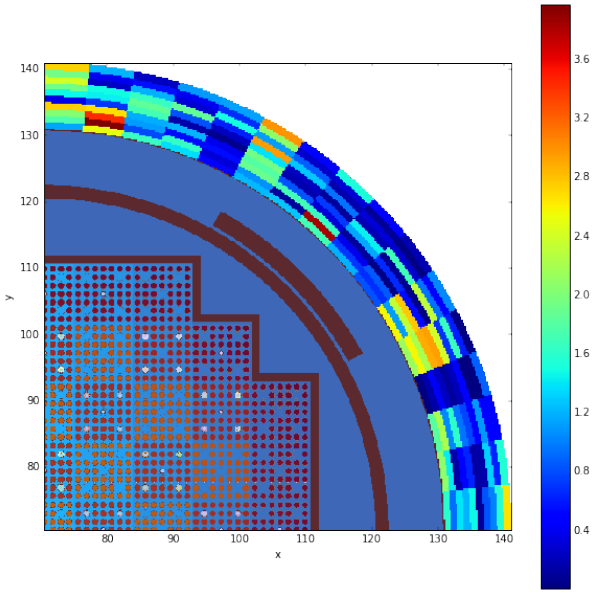

Figure 4.9 Assembly-averaged homogenization relative differences (%)

The relative differences, shown in Fig. 4.9, appear to be randomly distributed throughout the reactor pressure vessel. For this case, the maximum, minimum, absolute average, and average differ-

ences were 28.99%, -25.94%, 1.30%, and -0.331%, respectively. Assembly-averaged homogenization appears to agree well with the explicit temperature model and the differences are inline with the baseline values shown in Table 4.1. Assembly-averaged homogenization also appears to be significantly more accurate than the nonunique configuration; compared to the explicit temperature and density model.

Another homogenization considered was a single temperature and density ring encompassing the entire reactor core. The relative differences in vessel fluence, taken at the core midplane, for this case are shown in Fig. 4.10.

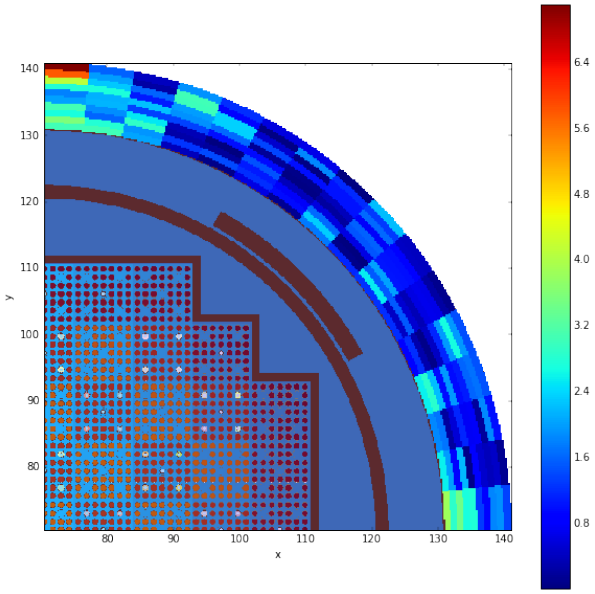

Figure 4.10 Single ring homogenization relative differences (%)

The relative differences, shown in Fig. 4.10, appear to be randomly distributed throughout the reactor pressure vessel and slightly higher than assembly-averaged homogenization. For this case, the maximum, minimum, absolute average, and average differences were 27.76%, -18.92%, 1.46%, and 0.197%, respectively. This homogenization appears to differ slightly from the explicit temperature model and the average differences are greater than the baseline values shown in Table 4.1. While the homogenization differed slightly from the explicit vessel fluence calculation, it was significantly more accurate than the nonunique configuration; compared to the explicit temperature and density model.

The remaining difference plots are shown in Appendix C.2. All of these cases performed similarly to Fig. 4.9 and Fig. 4.10. Diagnostics for these calculations are shown in Table 4.3.

Table 4.3 Homogenization Comparisons

Case	Maximum	Minimum	Average	Absolute Average
svs_exassem	28.74	-23.90	-0.175	1.30
svs_exassem2	42.48	-26.21	-0.261	1.27
svs_ex1ring	46.01	-20.30	-0.017	1.29
svs_assemring	81.82	-20.55	0.042	1.36
svs_pinring	88.64	-32.61	-0.106	1.30
svs_pinring2	52.20	-27.07	0.161	1.35
svs_exring	65.76	-21.49	-0.039	1.35
svs_exring2	200.4	-20.96	0.113	1.42
svs_multiring	45.02	-21.88	-0.215	1.25

While none of the average differences were significantly higher than the baseline from Table 4.1, the relative differences in vessel fluence were very inconsistent for ring homogenizations depending on the location and thickness of the rings. These differences were especially noticeable for pin- rings. The highest difference shown in Table 4.3 corresponds to svs_exring2. This homogenization had the highest average difference and largest maximum difference by a wide margin. It was hypothesized that these large discrepancies in vessel fluence for pin-rings are caused by combining pincells of different enrichments into the same temperature average.

Overall, these homogenizations performed well in vessel fluence calculations when compared to an explicit temperature model. Even with small discrepancies, all of the homogenizations considered, performed significantly better than the nonunique configuration.

Enrichment Investigation

As shown in the previous section, the effectiveness of the pin-ring homogenization varied greatly depending on the size and location of the ring boundaries. It is hypothesized that these differences are caused by averaging temperatures and densities of pincells with various enrichments together. This makes a much bigger difference for pin-rings than assembly-rings since the enrichments are consistent across assemblies and vary radially through the core. In order to investigate if these differences are caused by varying enrichments, we will consider a model identical to the mini-core, but with uniform enrichments throughout.

In this study we looked at four homogenizations detailed in Table 3.6. The relative difference in vessel fluence at the midplane of the reactor is included in Appendix C.3. These homogenizations were compared to an explicit core model using uniform enrichment. Diagnostics for these calculations are shown in Table 4.4.

Table 4.4 Enrichment Investigation

Case	Maximum	Minimum	Average	Absolute Average
enrich_assem	27.04	-49.68	-0.422	1.21
enrich_pinring	37.77	-49.99	-0.358	1.28
enrich_expinring	27.28	-42.93	-0.368	1.18
enrich_expinring2	39.52	-43.79	-0.253	1.16

Overall, the results shown in Table 4.4 showed very good agreement between the homogenizations and explicit solution. The average relative differences in vessel fluence are noticeably lower than the realistic enrichment cases. Additionally, there is far less variability in the accuracy of pin-ring homogenizations. The average relative difference decreases as more explicit peripheral pins are used. This is the expected behavior; seen using assembly homogenization, but not ring homogenization for the varying enrichment cases.

This investigation provides evidence that varying enrichments should be considered when defining homogenization regions. The impact was especially noticeable for pin-ring homogenization. While the impact is not massive, it should certainly be a consideration moving forward.

AMA Problem 7 Quarter-Core

Due to memory limitations, a fully unique solution could not be calculated for use as a benchmark. Instead, the most accurate, achievable, homogenization was selected as the benchmark solution. Due to issues with the inconsistency of pin-ring homogenizations, likely due to homogenizing different enrichments together, assembly-averaged homogenization was selected as the benchmark solution. This homogenization performed well in the mini-core investigation and accurately modeled differing enrichments throughout the core. Explicit peripheral pins were not investigated for the AMA Problem 7 configuration due to memory restrictions.

A 2D, radial, depiction of the reactor pressure vessel neutron fluence, at the reactor midplane, is shown in Fig. 4.11. Fig. 4.12 shows the axial pressure vessel neutron fluence radially through the pressure vessel; taken at $\theta = \frac{\pi}{2}$.

As anticipated, the vessel fluence peaked in the corner of the reactor; behind the pad. As a Monte Carlo calculation, all fluence tallies have an associated uncertainty. This uncertainty is important for determining the accuracy of the results; especially when comparing to other results. Fig. 4.13 shows the relative standard deviation of each tally presented in Fig. 4.11.

Most of the uncertainties in Fig. 4.13 are at or below 3%. These lower uncertainties were achiev-

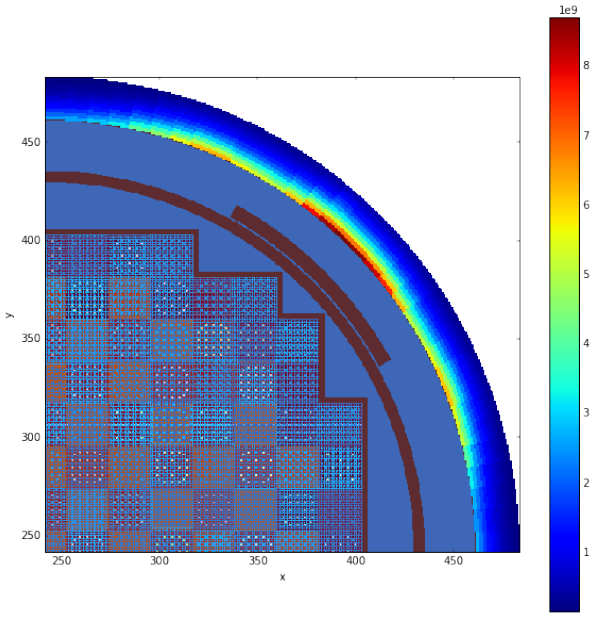

Figure 4.11 Quarter-core radial neutron fluence (n/cm^2)

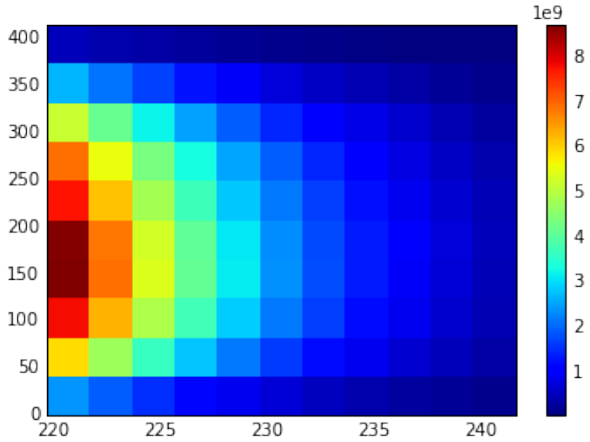

Figure 4.12 Quarter-core axial neutron fluence (n/cm^2)

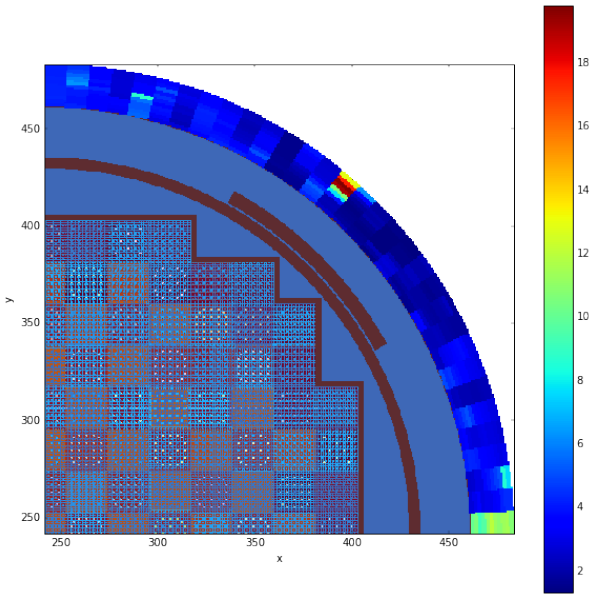

Figure 4.13 Quarter-core pressure vessel neutron fluence uncertainty (%)

able due to the addition of source biasing within CADIS. This was not used for the mini-core models.

An important consideration for this investigation is how each homogenization performs compared to the nonunique pincell configuration. Prior to this work, nonunique pincells were the only method for vessel fluence calculations with a realistic reactor geometry. Nonunique pincells represents a core approximation with no temperature, density or isotopics transfer. The relative differences for this case are shown in Fig. 4.14.

For this case, the maximum, minimum, absolute average, and average differences, over all axial levels, were 128.75%, -54.63%, 17.11%, and -16.94%, respectively. It is clear from the average differences that the nonunique vessel fluence is significantly different than the assembly-averaged homogenization model. Additionally, the vessel fluence calculated using nonunique pincells is shifted lower as evidenced by the absolute average difference. This means the nonunique solution is not only inaccurate, but also non-conservative.

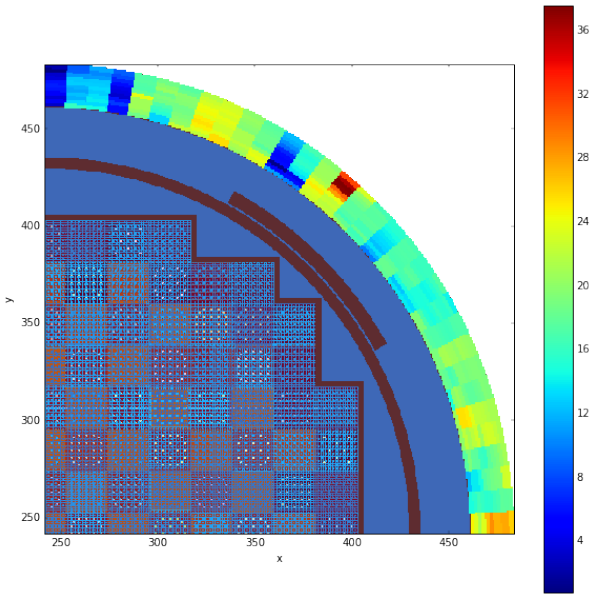

Figure 4.14 Nonunique pincell configuration relative differences(%)

Homogenization Investigation

In order to determine the accuracy of various homogenizations, a number of cases using different homogenizations were compared to an assembly-averaged temperature and density homogenization. Fuel temperature plots for each homogenization are presented in Appendix B.2. This evaluation was performed using semi-unique pincells. The first case that was considered was a single temperature and density ring homogenization. The relative differences in vessel fluence, taken at the core midplane, for this case are shown in Fig. B.13.

The relative differences, shown in Fig. 4.15, appear to be randomly distributed throughout the reactor pressure vessel; with a few very high uncertainties in the eastern and north-eastern portions of the core. For this case, the maximum, minimum, absolute average, and average differences, over all axial levels, were 118.76%, -48.06%, 4.57%, and 0.973%, respectively. A single temperature ring homogenization appears to be significantly more accurate than the nonunique configuration.

The second case that was considered was a assembly-ring averaged temperature and density homogenization. The relative differences in vessel fluence, taken at the core midplane, for this case are shown in Fig. 4.16.

The relative differences, shown in Fig. 4.16, appear to be randomly distributed throughout the reactor pressure vessel; with a few very high differences in the northern and eastern portions of the core. For this case, the maximum, minimum, absolute average, and average differences, over all axial levels, were 120.23%, -42.58%, 4.35%, and -0.171%, respectively. The assembly-ring homogenization

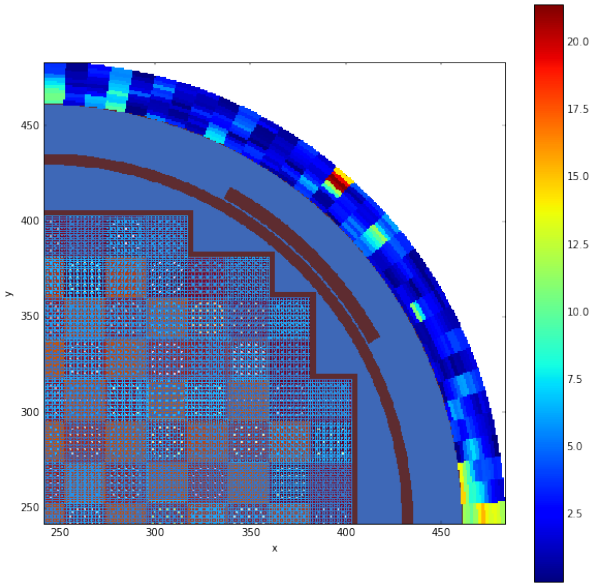

Figure 4.15 Single ring homogenization relative differences (%)

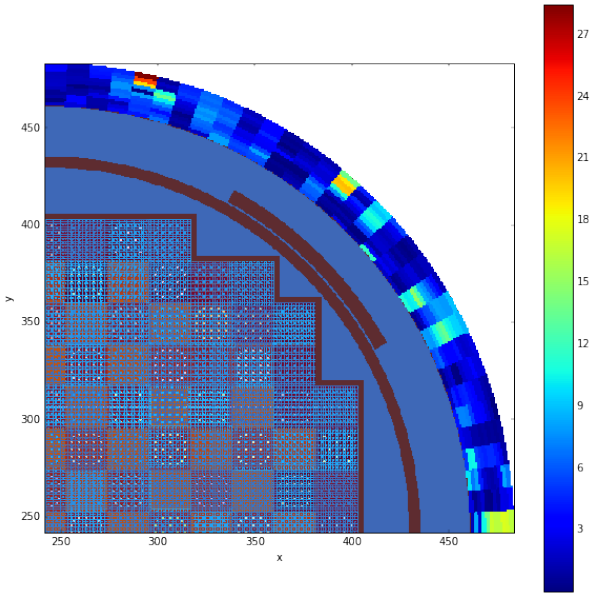

Figure 4.16 Assembly-ring homogenization relative differences (%)

appears to be significantly more accurate than the nonunique configuration.

The third case that was considered was a coarse, pin-ring averaged temperature and density homogenization. The relative differences in vessel fluence, taken at the core midplane, for this case are shown in Fig. 4.17.

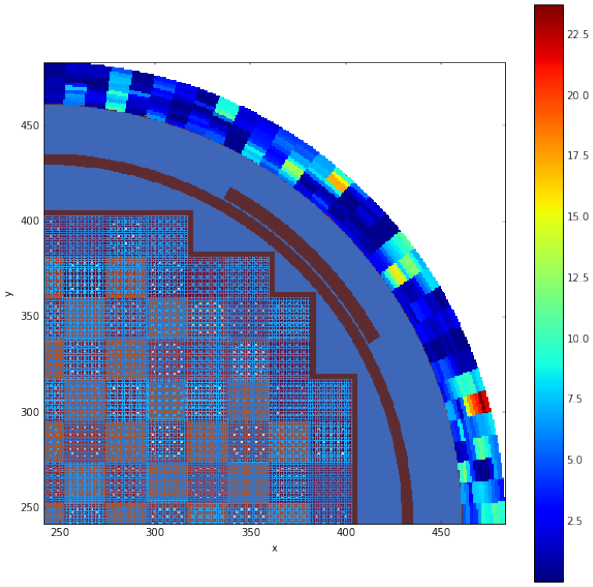

Figure 4.17 Coarse pin-ring homogenization relative differences (%)

The relative differences, shown in Fig. 4.17, appear to be randomly distributed throughout the reactor pressure vessel with a few high differences in the eastern portions of the core. For this case, the maximum, minimum, absolute average, and average differences, over all axial levels, were 526.53%, -45.21%, 7.47%, and 3.837%, respectively. This homogenization performed the worst; possibly due to one extremely high difference of 526%. This difference could have led to the high differences in average and absolute average difference. Other than the high maximum difference, The coarse pin-ring homogenization appears to be significantly more accurate than the nonunique configuration.

The fourth case that was considered was a medium, pin-ring averaged temperature and density homogenization. The relative differences in vessel fluence, taken at the core midplane, for this case are shown in Fig. 4.18.

The relative differences, shown in Fig. 4.18, appear to be randomly distributed throughout the reactor pressure vessel. For this case, the maximum, minimum, absolute average, and average differences, over all axial levels, were 72.77%, -46.54%, 4.73%, and 1.26%, respectively. The

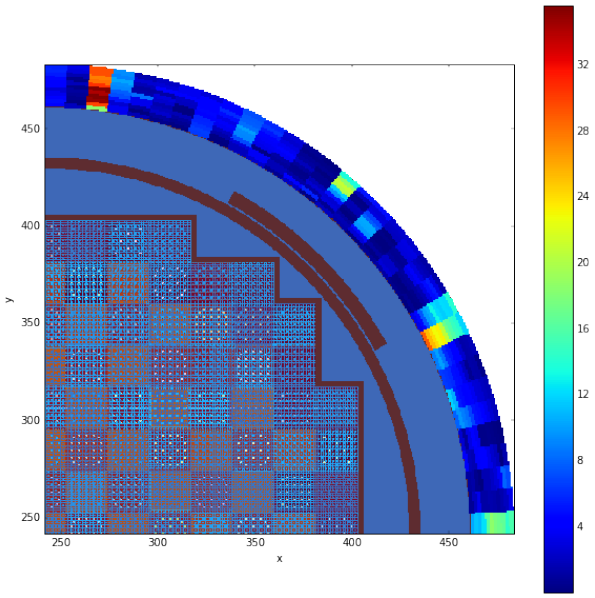

Figure 4.18 Medium pin-ring homogenization relative differences (%)

medium pin-ring homogenization appears to be significantly more accurate than the nonunique configuration.

The fifth case that was considered was a fine, pin-ring averaged temperature and density homogenization. The relative differences in vessel fluence, taken at the core midplane, for this case are shown in Fig. 4.19.

The relative differences, shown in Fig. 4.19, appear to be randomly distributed throughout the reactor pressure vessel. For this case, the maximum, minimum, absolute average, and average differences, over all axial levels, were 104.75%, -43.36%, 4.76%, and 0.861%, respectively. The fine pin-ring homogenization appears to be significantly more accurate than the nonunique configuration.

Overall, the AMA Problem 7 quarter full-core results appear to be very promising. It is difficult to differentiate the performance of each individual homogenization with high uncertainties and no true benchmark solution. However, all of the homogenizations tested performed significantly better than the nonunique pincell configuration.

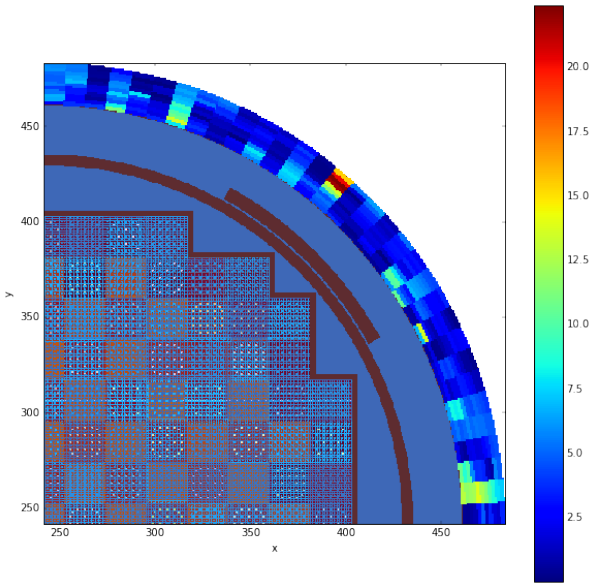

Figure 4.19 Fine pin-ring homogenization relative differences (%)

Performance Enhancement

The ultimate goal of these core approximations, was to reduce the computational expense of vessel fluence calculations; while maintaining sufficient accuracy. These methods were developed with the intention of reducing memory usage for large problems. In addition to memory savings, these approximations led to runtime reductions for CADIS within VERAShift.

All cases were run on the CADES computing cluster at ORNL.

Memory Improvement

The core approximations were intended to reduce the memory costs of large vessel fluence calculations in Shift. These memory savings were achieved by using the new semi-unique, geometry configuration in Shift. Semi-unique pincells drastically reduce the number of unique geometry and material specifications in the core metadata; as described in Chapter 2. By reducing the size of the core metadata and reducing the number of unique cross section libraries, these core approximations can greatly reduce the Shift memory usage. The overall memory usage for various mini-core homogenizations are reported in Table 4.5. Table 4.6 presents the memory usage for quarter full-core homogenizations. The cases in Table 4.5 correspond to the homogenization comparisons described in Table 3.6 and the cases in Table 4.6 correspond to the homogenizations described in Table 3.7.

Table 4.5 shows the memory usage for various homogenization methods. The memory usage varies greatly depending on which homogenization is being performed. As expected, basic assembly

Table 4.5 Total memory usage: mini-core

Case	Memory Usage(GB)
Unique Pincells	56.2
Nonunique Pincells	16.5
Semi-Unique	
Fully Explicit	49.9
svs_assem	29.9
svs_exassem	47.1
svs_exassem2	48.9
svs_1ring	23.0
svs_assemring	27.1
svs_pinring	30.1
svs_exring	46.0
svs_exring2	49.1
svs_ex1ring	46.5
svs_multiring	30.0
svs_pinring2	26.8

Table 4.6 Total memory usage: quarter full-core

Case	Memory Usage(GB)
Nonunique Pincells	52.5
Assembly	90.7
One Ring	68.3
Assembly Ring	81.1
Coarse Ring	78.7
Medium Ring	83.8
Fine Ring	90.2

and ring homogenizations showed the greatest reduction in memory usage; with a single temperature and density across the entire core using the least memory. Assembly and ring homogenizations dramatically reduced the memory usage compared to unique pincells; up to a factor of 2-3 reduction. All semi-unique pincell cases used less memory than the unique pincell problem. The use of explicit peripheral temperature and density modeling greatly increases the memory usage.

Similarly to Table 4.5, Table 4.6 showed a substantial reduction in memory usage in the quarter full-core model for various homogenizations. Explicit pincells were not considered in this investigation due to the large increase in memory usage. The most detailed homogenization, assembly-averaged, used nearly 91GB out of a maximum 132GB. Compared to assembly homogenization, a single temperature and density ring used only 75% the memory.

Overall, the core approximations offered moderate to significant memory savings when compared to unique pincell configuration. Memory usage increases quickly with more detail in the homogenization; especially with the use of explicit peripheral pincells. For the quarter full-core model, temperature and density homogenization with semi-unique pincells reduced memory usage; enabling more detailed models than previously capable.

Runtime Reduction

In addition to reducing memory usage, minor improvements were anticipated in Shift runtimes; when using CADIS. Simplifying the reactor model was expected to reduce the time needed for the deterministic code to converge. The reported runtime includes the time for the CADIS calculation and the Monte Carlo transport with 10^8 neutrons for mini-core and 10^{10} neutrons for quarter full-core. The total Shift runtime for various mini-core homogenizations is reported in Table 4.7. Table 4.6 presents the Shift runtime for quarter full-core homogenizations. The cases in Table 4.7 correspond to the homogenization comparisons described in Table 3.6 and the cases in Table 4.8 correspond to the homogenizations described in Table 3.7.

Table 4.7 shows significant decreases in Shift runtimes for various mini-core homogenizations. These differences were much larger than expected and showed a dramatic improvement over the unique pincell calculation. The simplest homogenization, a single temperature and density ring, had the shortest runtime; just over $\frac{1}{6}$ the time of the unique pincell calculation. Assembly and ring homogenizations dramatically reduced the Shift calculation runtime compared to unique pincells; up to a factor of 3-4 reduction. All semi-unique pincell cases were faster than the unique pincell calculation. The use of explicit peripheral temperature and density modeling greatly increases the runtime.

Similarly to Table 4.7, Table 4.8 showed significant runtime improvement for various homogenization methods for the AMA Problem 7 quarter full-core model. Generally, as the number of homogenization regions increases, the Shift runtime increases.

Table 4.7 Shift runtime: mini-core

Case	Shift Runtime(s)
Unique Pincells	98.6
Nonunique Pincells	9.45
Semi-Unique	
Fully Explicit	96.9
svs_assem	28.7
svs_exassem	87.1
svs_exassem2	89.5
svs_1ring	18.2
svs_assemring	25.1
svs_pinring	60.9
svs_exring	85.9
svs_exring2	90.0
svs_ex1ring	86.7
svs_multiring	42.8
svs_pinring2	24.5

Table 4.8 Shift runtime: quarter full-core

Case	Shift Runtime(min)
Nonunique Pincells	180
Assembly	262
One Ring	210
Assembly Ring	250
Coarse Ring	236
Medium Ring	258
Fine Ring	301

Overall, the core approximations offered significant runtime savings when compared to unique pincell configuration. Runtime improvements were significantly greater than anticipated in this investigation. Runtime increases quickly with more detail in the homogenization; especially with the use of explicit peripheral pincells.

CHAPTER

5

CONCLUSIONS

The objective of this project was to develop new core approximation techniques for vessel fluence calculations. The method used in this project was volume-average, temperature and density homogenization. The two basic types of homogenization were assembly-averaged and ring-averaged. These core approximations were developed with the intent of reducing computational expense; without sacrificing accuracy. Temperature and density homogenization was shown to reduce memory usage by up to a factor of 2-3 and decreased runtime by up to a factor of 5; using the mini-core configuration.

Prior to this work, Shift had two geometry configurations; unique and nonunique pincells. Semi-unique pincells were created to enable temperature and density homogenization without uniquely specifying material and geometry properties at every location in the core. The accuracy of the semi-unique pincells was tested against the results using unique pincells for the mini-core geometry configuration. In all cases considered, other than assembly-ring homogenization, the differences between semi-unique and unique pincells were within the expected range from the stochastic nature of Monte Carlo calculations. For the assembly-ring homogenization high differences were observed in a single theta bin of the vessel fluence tally. These differences were not observed in any other cases and could have been caused by random differences between the cases.

The accuracy of various homogenizations were investigated by comparing to a model using explicit temperature and density modeling. For the mini-core configuration, all homogenizations significantly outperformed the nonunique pincell solution. Most of the homogenizations performed

very well. Using a single temperature and density ring appeared to be less accurate than other homogenizations, but had the least memory usage and shortest Shift runtime. Pin-ring homogenizations performed inconsistently depending on the thickness and locations of the rings. It was shown that varying enrichments throughout the core could contribute to this observation and consideration should be taken when defining ring boundaries.

In addition to the mini-core geometry, we considered a AMA Problem 7 quarter full-core geometry. Due to memory limitations, homogenizations were compared to the most accurate homogenization that could be simulated for a realistic core geometry. The assembly homogenization was selected due to the consistently accurate results in the mini-core. Due to relatively high uncertainty, it was difficult to differentiate the impact of different homogenization. However, it was clear that all homogenizations out-performed nonunique pincells.

Overall, the results of this project were extremely promising. Temperature and density homogenization using semi-unique pincells was shown to significantly reduce computational expense without sacrificing accuracy.

Moving forward, it is important to benchmark these temperature and density homogenization methods against an explicit model for a realistic reactor geometry. Due to memory restrictions, it is not possible to perform vessel fluence calculations with fully explicit temperature and density for a full core reactor model. This is essential for understanding the accuracy of these core approximation in a realistic problem.

While the results of this project were very promising, there are a number of improvements that can be made in the future. Currently only temperatures and densities are transferred when using semi-unique pincells. In order to perform depletion calculations, isotopic transfer must be enabled. Due to each pincell not being uniquely defined, some form of homogenization would be necessary for material number densities.

During this project, it was determined that lumping differing enrichments into the same homogenization region can lead to inaccuracies in vessel fluences calculations. In order to prevent this, homogenizations can be adjusted to homogenize each fuel enrichment separately. This would also be beneficial in implementing isotopics transfer.

BIBLIOGRAPHY

[1] *Calculational and dosimetry methods for determining pressure vessel neutron fluence. Regulatory Guide 1.190*. Nuclear Regulatory Commission. 2001.

[2] Collins, B. et al. *MPACT Theory Manual*. CASL-U-2015-0078-000. Version 2.0.0. CASL. 2015.

[3] Godfrey, A. *VERA Core Physics Benchmark Progression Problem Specifications*. CASL-U-2012-0131-004. 2014.

[4] Godfrey, A. "Status Report: Watts Bar Nuclear Unit 2 Startup and Simulation". PowerPoint Presentation. 2016 Round Table Meeting, Sandia National Labratory, 2016.

[5] *HDF5: API Specification Reference Manual*. Version 1.10. The HDF Group. 2017.

[6] Johnson, S. et al. *Exnihilo Transport Code Manual*. Oak Ridge National Laboratory. 2017.

[7] *MCNP - A General Monte Carlo N-Particle Transport Code*. LA-13709-M. Los Alamos National Laboratory. 2000.

[8] Montgomery, R. *VERA Tools and Workflows. Revision 1*. CASL-U-2014-0051-001. CASL. 2014.

[9] Palmtag, S & Godfrey, A. *VERA Common Input User Manual*. CASL-U-2012-0131-004. CASL. 2014.

[10] Pandya, T. et al. "Implementation, capabilities, and benchmarking of Shift, a massively parallel Monte Carlo radiation transport code". *Journal of Computational Physics* **308** (2016), pp. 239–272.

[11] Pandya, T. et al. *Excore Radiation Transport Modeling with VERA*. CASL-U-2017-1311-001. CASL. 2017.

[12] Pavinich, W. *Analysis of Capsule W from the Tennessee Valley Authority Watts Bar Unit 1 Reactor Vessel Material Surveillance Program*. BWXT Services, Inc. 2001.

[13] Peplow, D. et al. *Consistent Adjoint Driven Importance Sampling Using Space, Energy and Angle*. ORNL/TM-2012/7. ORNL. 2012.

[14] Rhoades, W. & Childs, R. *An Updated Version of the DORT One- and Two-Dimensional Neutron/Photon Transport Code*. ORNL-5851. Oak Ridge National Laboratory. 1982.

[15] Salko, R. & Avramova, M. *CTF Theory Manual*. NC State University. 2018.

[16] Slattery, S. & Wilson, P. "The Data Transfer Kit: A Geometric Rendezvous-Based Tool for Multiphysics Data Transfer". M&C 2013. American Nuclear Society. 2013.

[17] Wagner, J. et al. “Monte Carlo Transport Calculations and Analysis for Reactor Pressure Vessel Neutron Fluence”. *Nuclear Technology* **114**.3 (1996), pp. 373–398.

APPENDICES

APPENDIX

A

MATERIAL SPECIFICATIONS

AMA Problem 7 - Material Specifications

Table A.1 AMA problem 7: 2.1% Enriched Fuel

Isotope	**Weight Density (g/cm^3)**
U^{238}	$8.62657e-01$
U^{235}	$1.85998e-02$
U^{234}	$1.65538e-04$
U^{236}	$8.55592e-05$
O^{16}	$1.18492e-01$

Table A.2 AMA problem 7: 2.6% Enriched Fuel

Isotope	**Weight Density (g/cm^3)**
U^{238}	$8.58103e-01$
U^{235}	$2.30865e-02$
U^{234}	$2.0547e-04$
U^{236}	$1.06198e-04$
O^{16}	$1.18499e-01$

Table A.3 AMA problem 7: 3.1% Enriched Fuel (g/cm^3)

Isotope	**Weight Density**
U^{238}	$8.538e-01$
U^{235}	$2.73263e-02$
U^{234}	$2.43204e-04$
U^{236}	$1.25701e-04$
O^{16}	$1.18505e-01$

Table A.4 AMA problem 7: Cladding

Isotope	Weight Density (g/cm^3)
Cr^{50}	$4.174e-05$
Cr^{52}	$8.370e-04$
Cr^{53}	$9.674e-05$
Cr^{54}	$2.453e-05$
Fe^{54}	$1.186e-04$
Fe^{56}	$1.930e-03$
Fe^{57}	$4.537e-05$
Fe^{58}	$6.143e-06$
Zr^{90}	$4.981e-01$
Zr^{91}	$1.098e-01$
Zr^{92}	$1.697e-01$
Zr^{94}	$1.757e-01$
Zr^{96}	$2.892e-02$
Sn^{112}	$1.326e-04$
Sn^{114}	$9.182e-05$
Sn^{115}	$4.772e-05$
Sn^{116}	$2.058e-03$
Sn^{117}	$1.097e-03$
Sn^{118}	$3.488e-03$
Sn^{119}	$1.248e-03$
Sn^{120}	$4.772e-03$
Sn^{122}	$6.894e-04$
Sn^{124}	$8.763e-04$
Hf^{174}	$1.559e-07$
Hf^{176}	$5.185e-06$
Hf^{177}	$1.844e-05$
Hf^{178}	$2.720e-05$
Hf^{189}	$1.366e-05$
Hf^{190}	$3.537e-05$

APPENDIX

B

HOMOGENIZATION CASES

Mini-Core

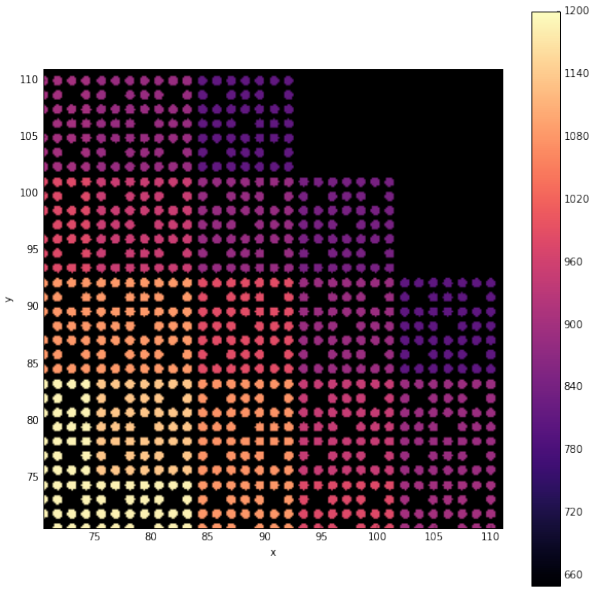

Figure B.1 svs_assem: fuel temperatures(K)

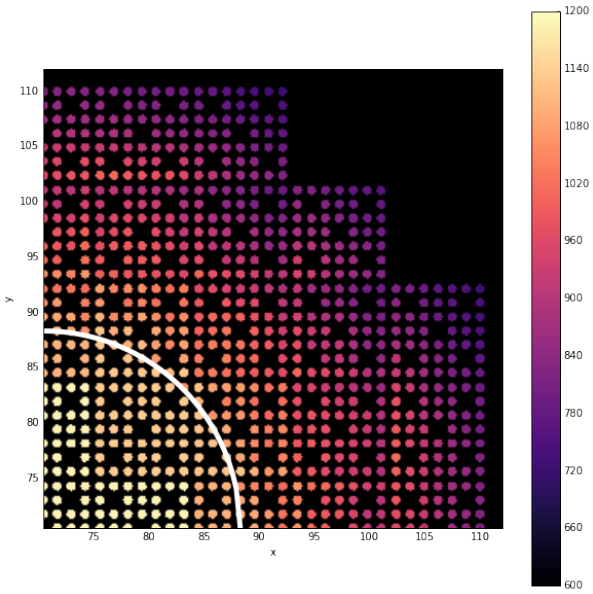

Figure B.2 svs_exassem: fuel temperatures(K)

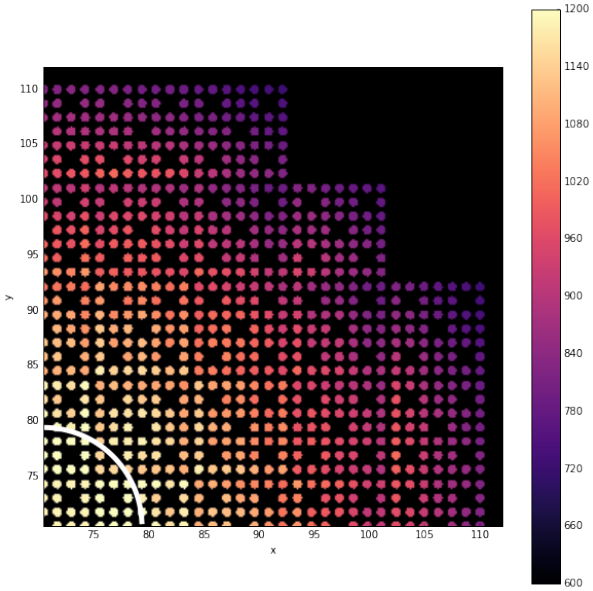

Figure B.3 svs_exassem2: fuel temperatures(K)

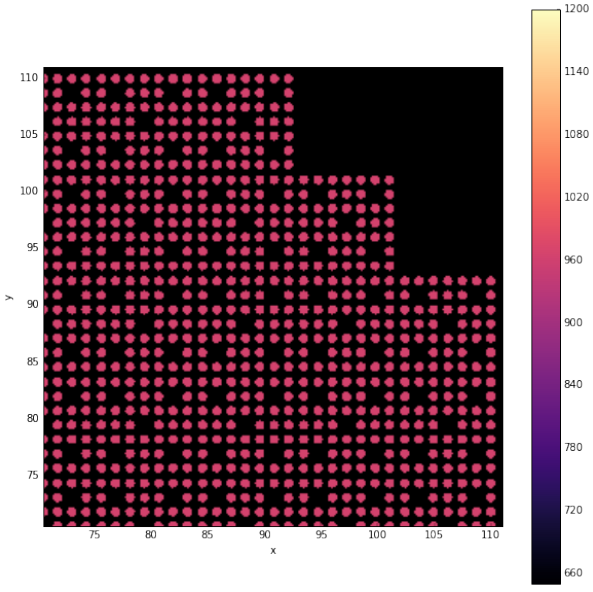

Figure B.4 svs_1ring: fuel temperatures(K)

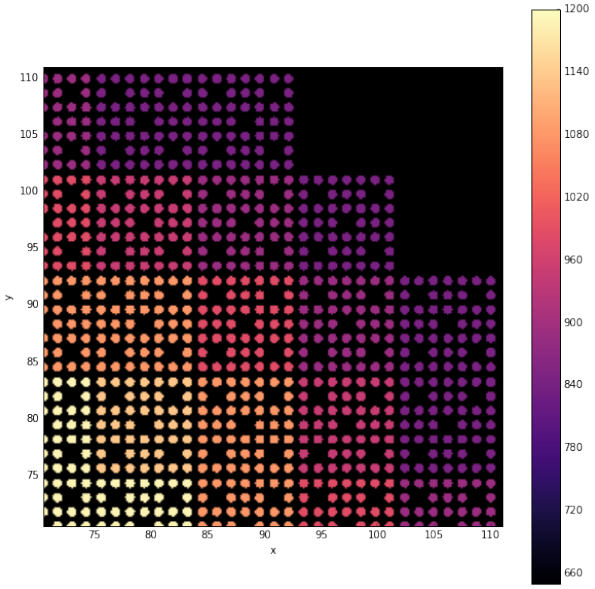

Figure B.5 svs_assemring: fuel temperatures(K)

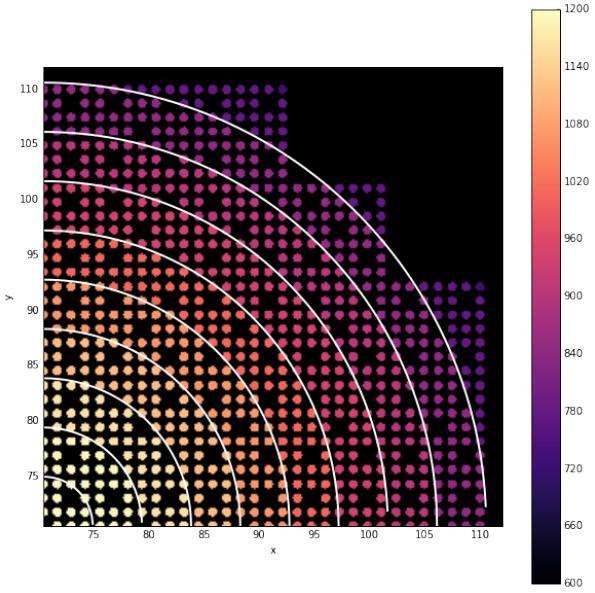

Figure B.6 svs_pinring: fuel temperatures(K)

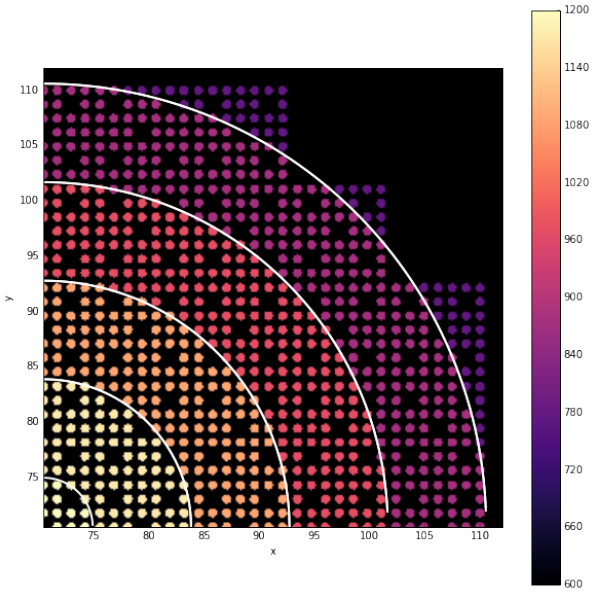

Figure B.7 svs_pinring2: fuel temperatures(K)

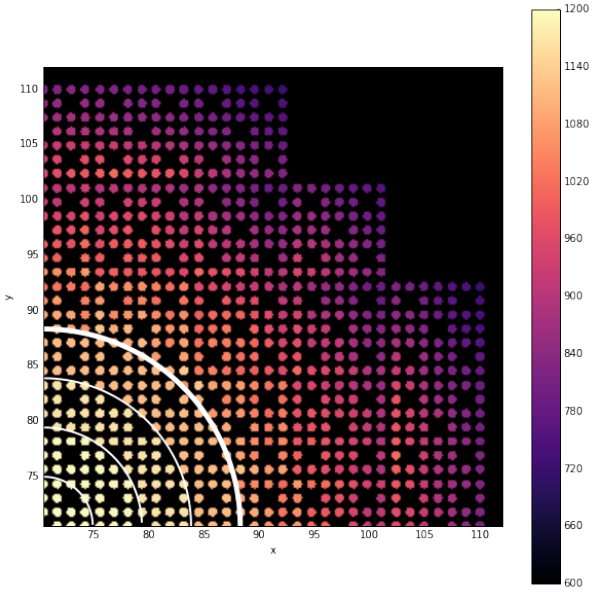

Figure B.8 svs_exring: fuel temperatures(K)

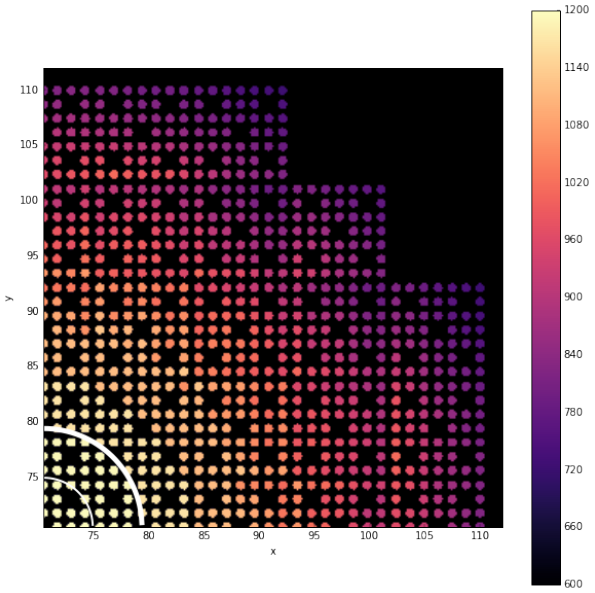

Figure B.9 svs_exring2: fuel temperatures(K)

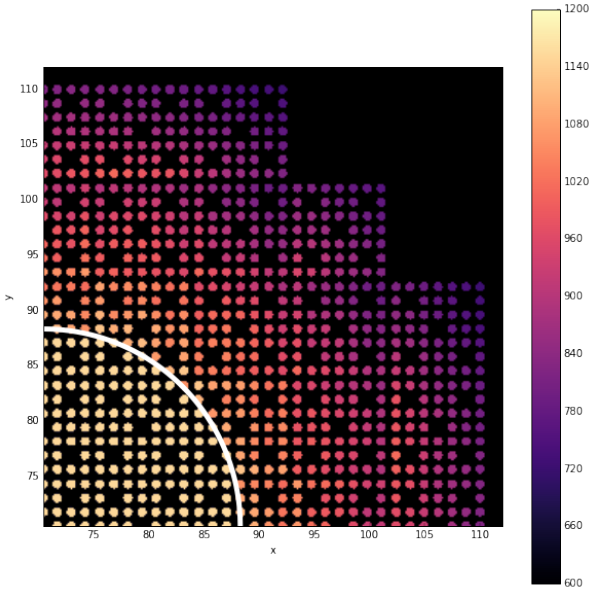

Figure B.10 svs_ex1ring: fuel temperatures(K)

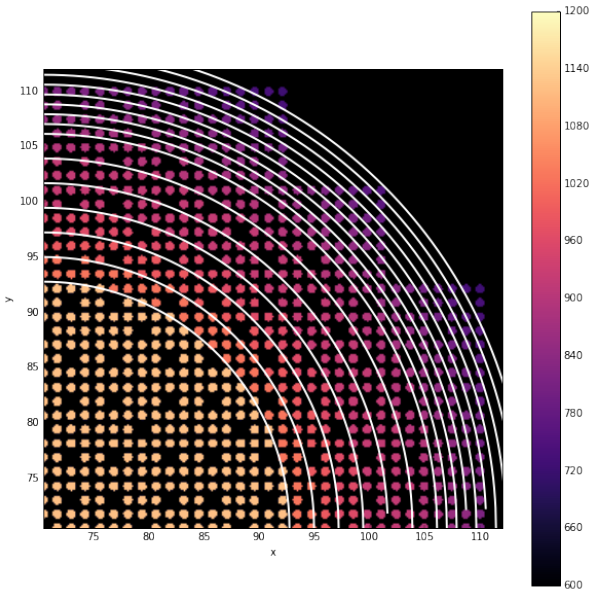

Figure B.11 svs_multiring: fuel temperatures(K)

Quarter Core

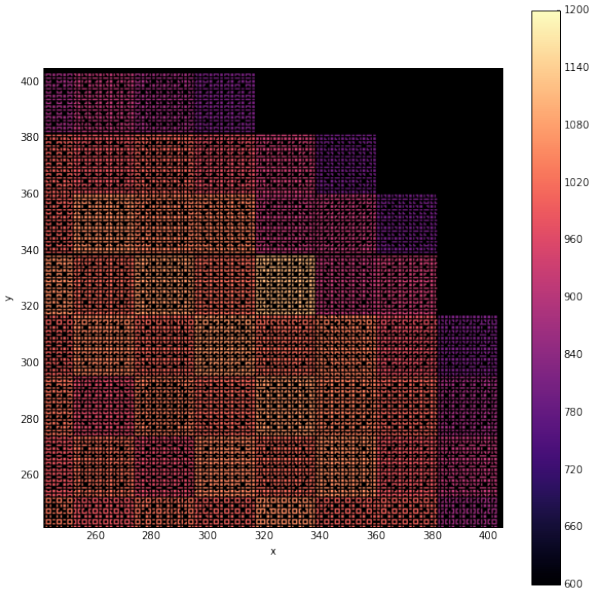

Figure B.12 Assembly: fuel temperatures(K)

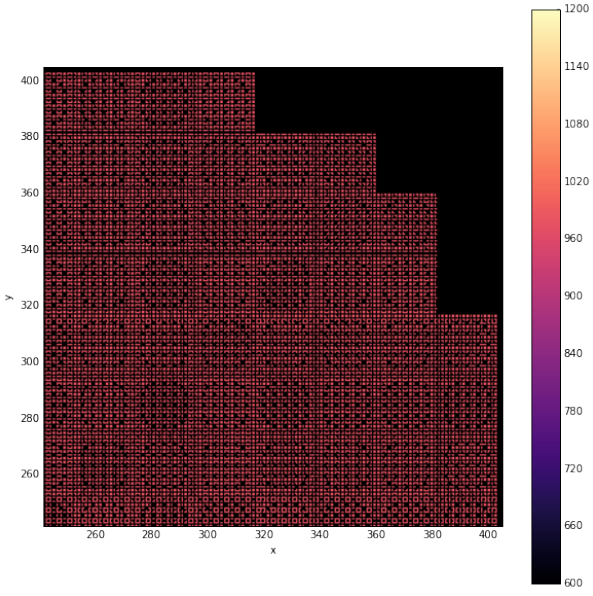

Figure B.13 One Ring: fuel temperatures(K)

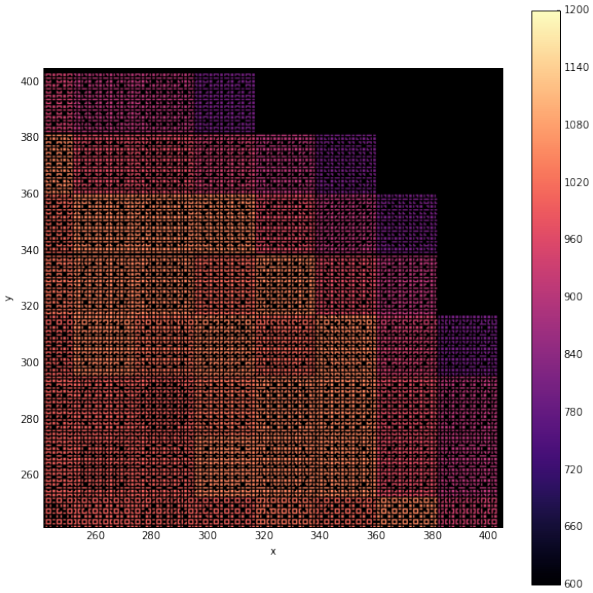

Figure B.14 Assembly Ring: fuel temperatures(K)

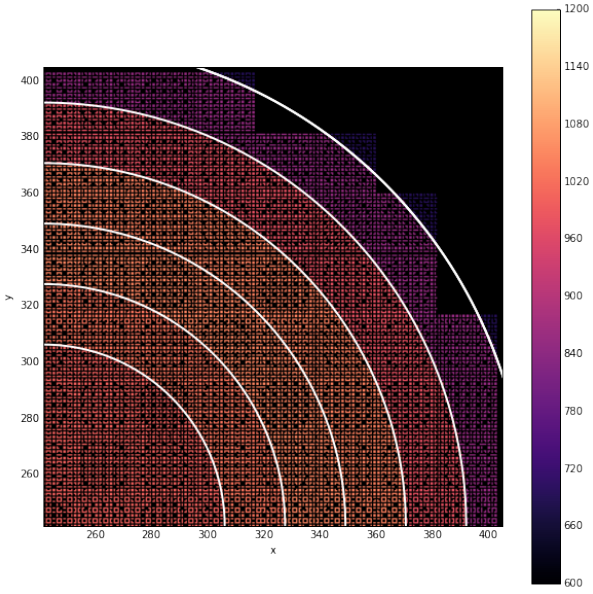

Figure B.15 Coarse Rings: fuel temperatures(K)

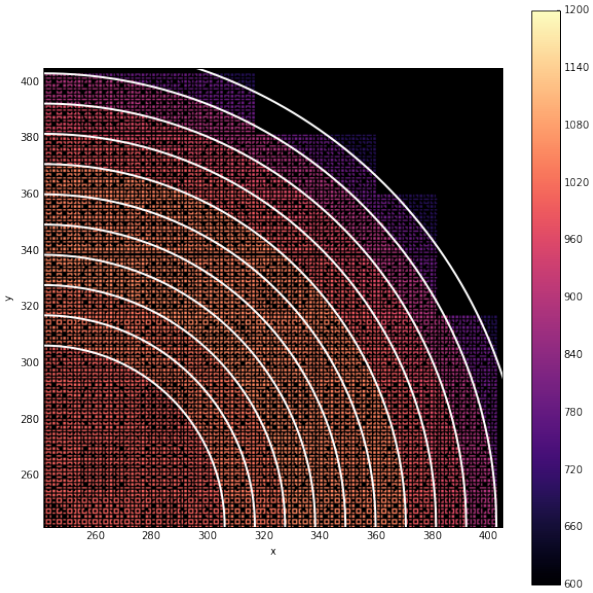

Figure B.16 Medium Rings: fuel temperatures(K)

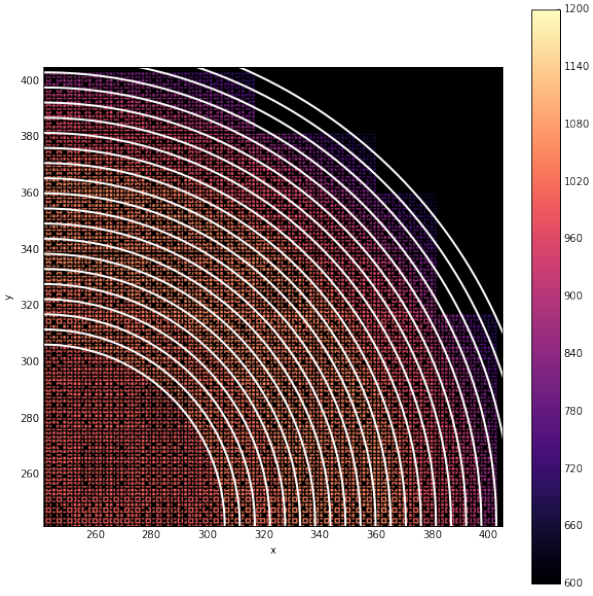

Figure B.17 Fine Rings: fuel temperatures(K)

APPENDIX

C

HOMOGENIZATION COMPARISION RELATIVE DIFFERENCES

Unique vs. Semi-Unique

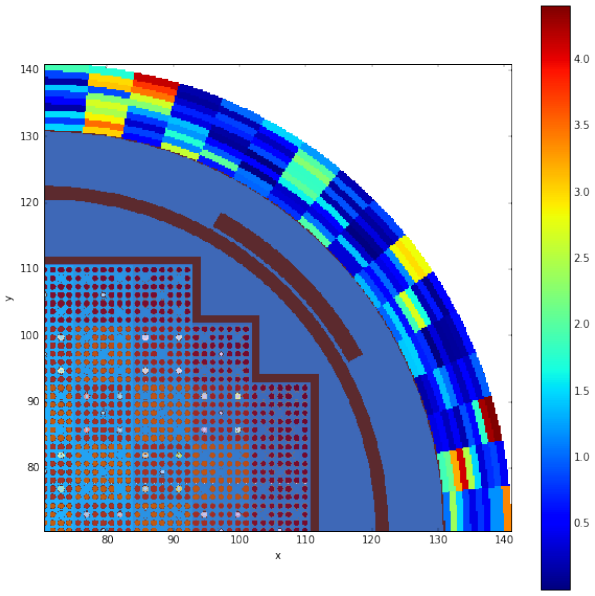

Figure C.1 uvs_exassem: relative differences (%)

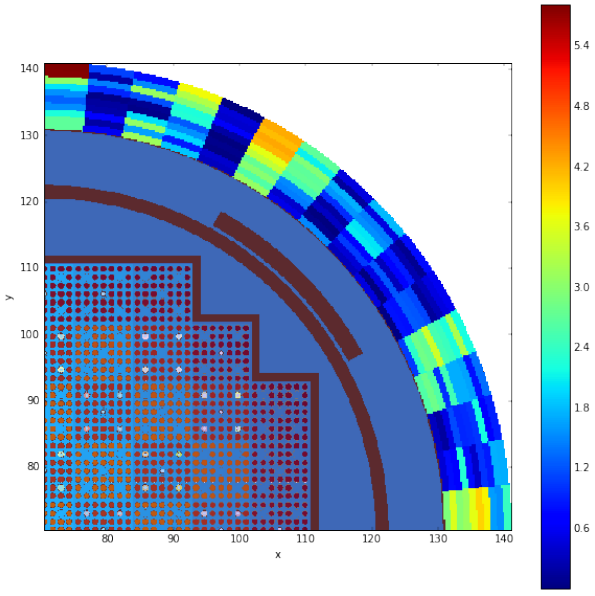

Figure C.2 uvs_1ring: relative differences (%)

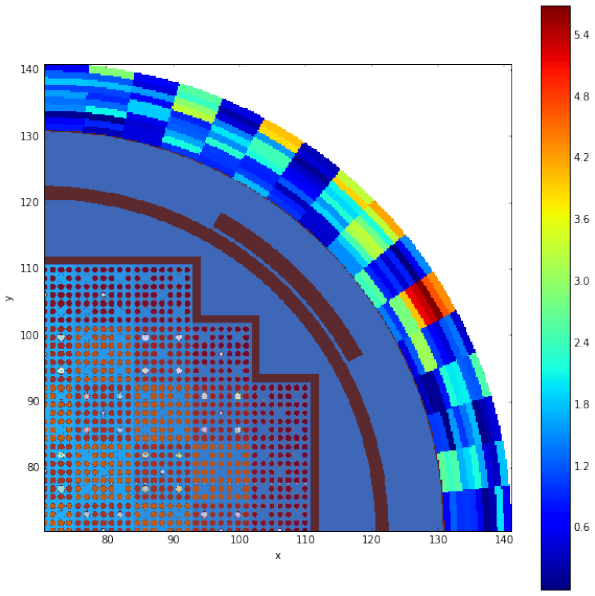

Figure C.3 uvs_ex1ring: relative differences (%)

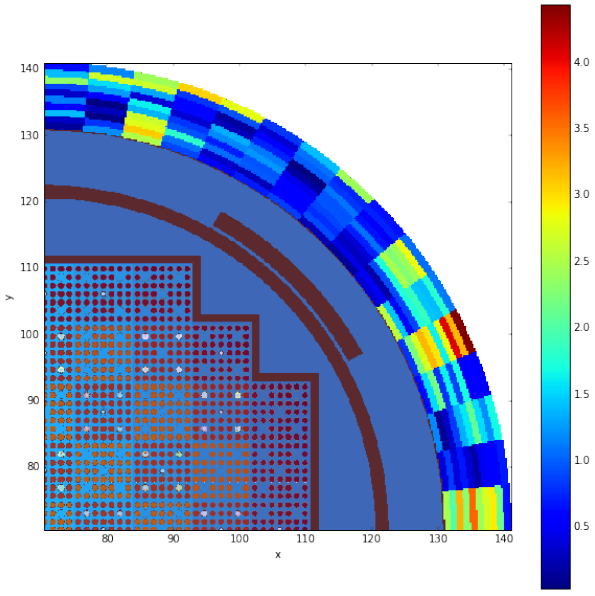

Figure C.4 uvs_pinring: relative differences (%)

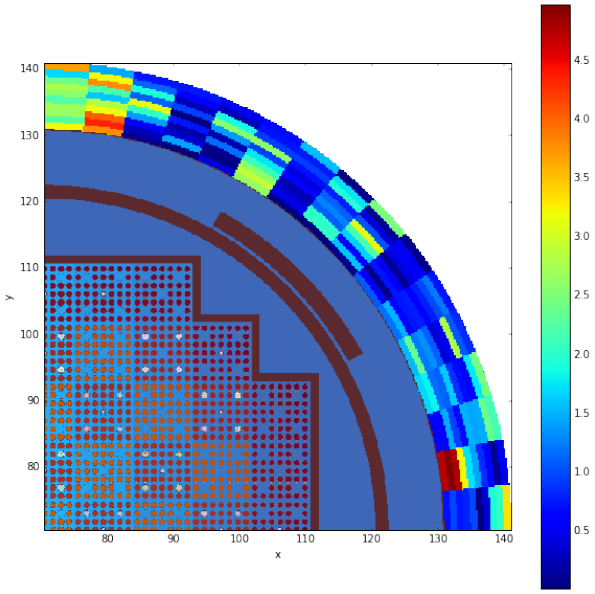

Figure C.5 svs_exassem: relative differences (%)

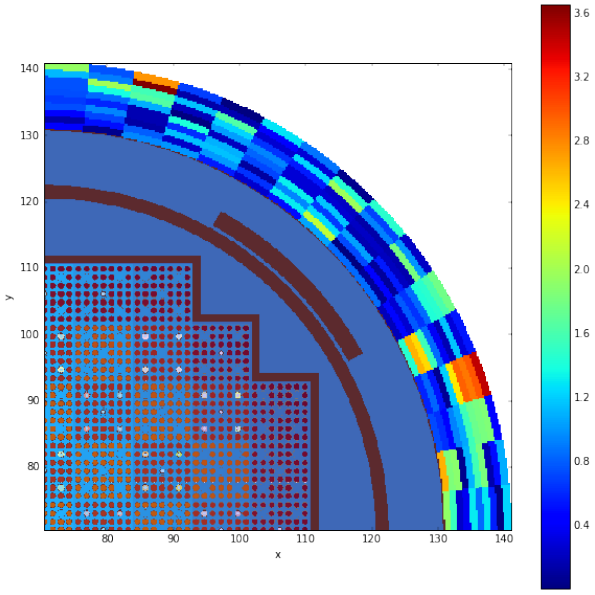

Figure C.6 svs_exassem2: relative differences (%)

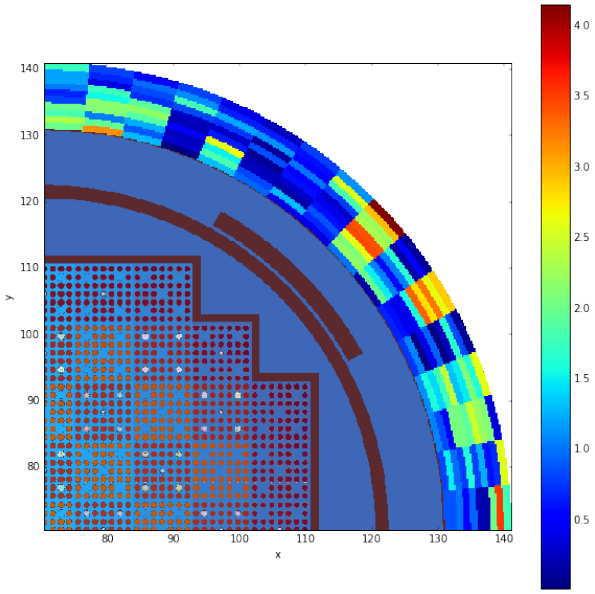

Figure C.7 svs_ex1ring: relative differences (%)

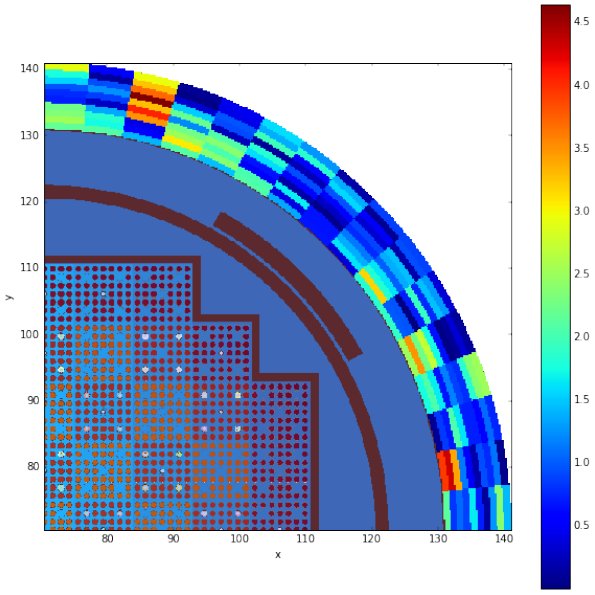

Figure C.8 svs_assemring: relative differences (%)

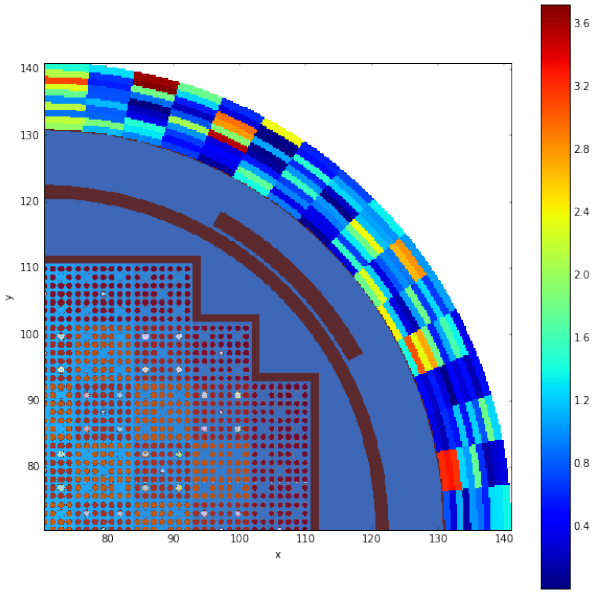

Figure C.9 svs_pinring: relative differences (%)

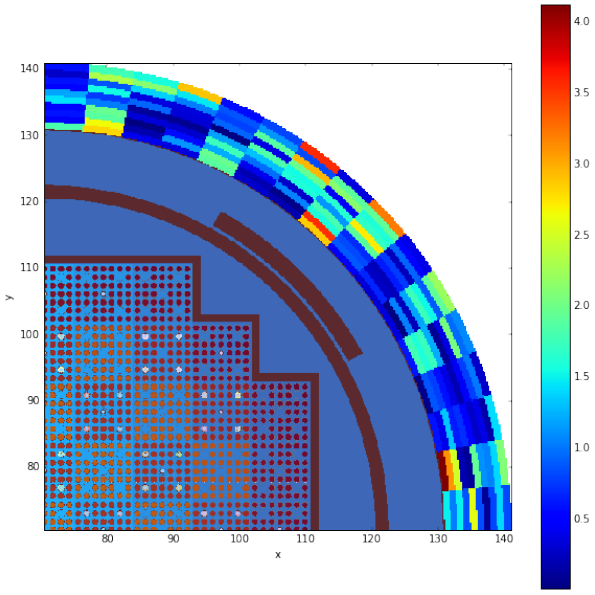

Figure C.10 svs_pinring2: relative differences (%)

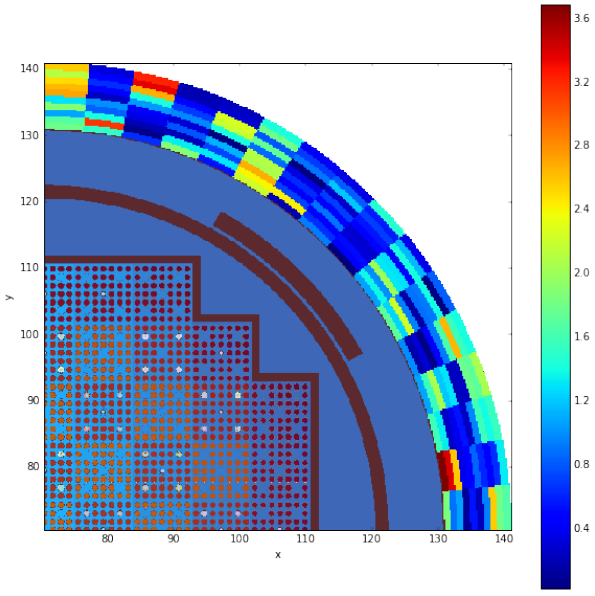

Figure C.11 svs_multiring: relative differences (%)

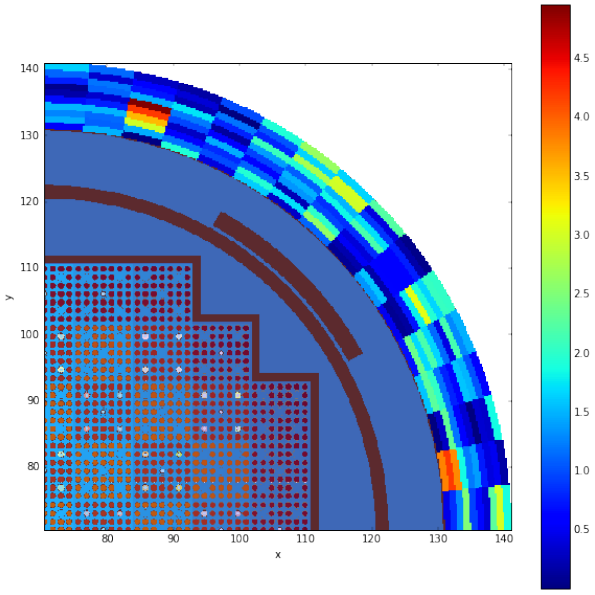

Figure C.12 svs_exring: relative differences (%)

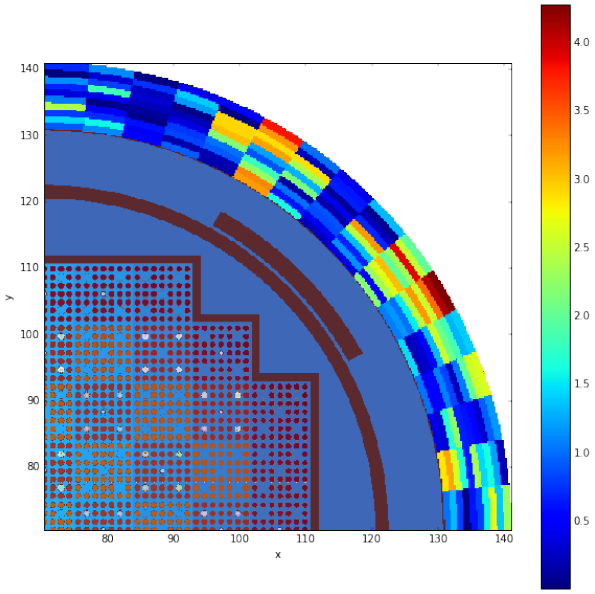

Figure C.13 svs_exring2: relative differences (%)

Enrichment Study

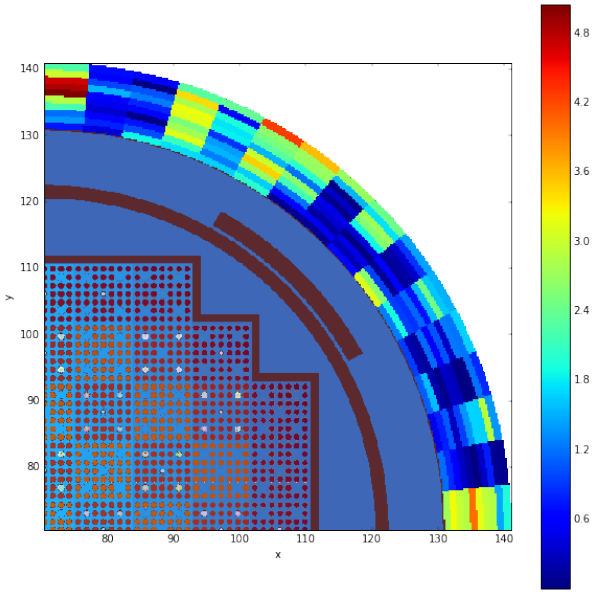

Figure C.14 enrich_assem: relative differences (%)

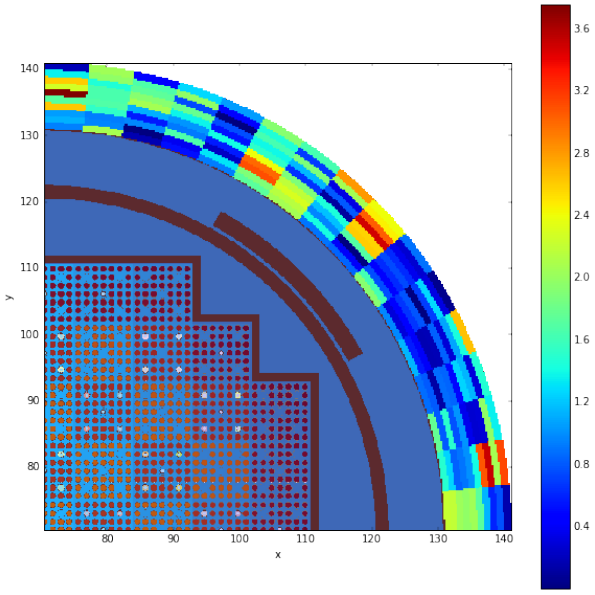

Figure C.15 enrich_pinring: relative differences (%)

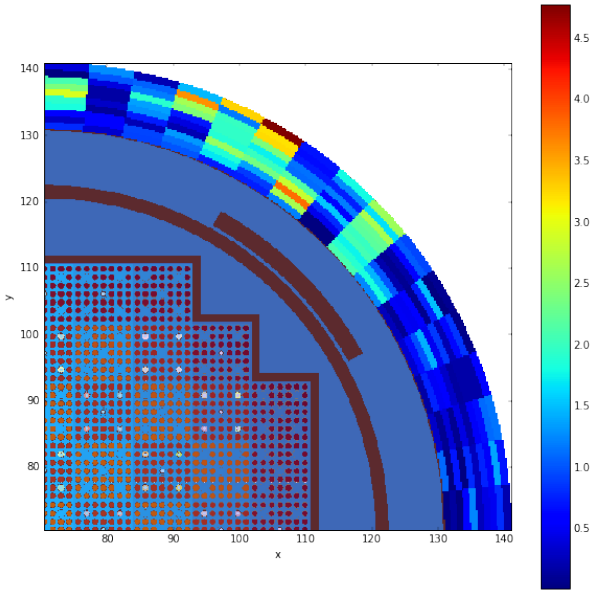

Figure C.16 enrich_pinring: relative differences (%)

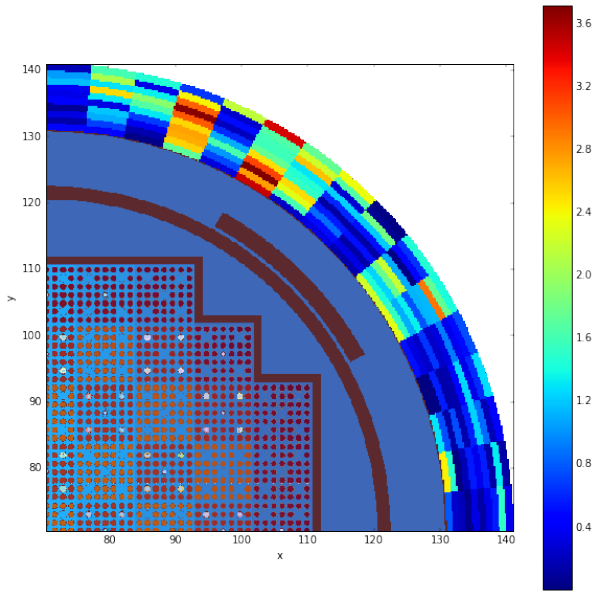

Figure C.17 enrich_pinring2: relative differences (%)